Indentation of Solid Nitrogen Between 30 K and 40 K

A Thesis

Presented in Partial Fulfillment of the Requirements for the

Degree of Master of Science

with a

Major in Mechanical Engineering

in the

College of Graduate Studies

University of Idaho

by

Zachary D. Hacker

Approved by:

Major Professor: Michael Maughan, Ph.D., P.E.

Committee Members: Robert Stephens, Ph.D., P.E.; Jacob Leachman, Ph.D.

Department Administrator: Gabriel Potirniche, Ph.D., P.E.

December 2021

Abstract

This research was completed in support of the proposed NASA mission, Triton Hopper, whose intended mission is to land on Triton, a moon of Neptune. Flight over Tritons surface is to be provided by repurposing in situ resources; where solidified nitrogen is gathered, heated, and used as a gaseous propellant. Mechanical property data of solid nitrogen at Triton surface conditions is almost nonexistent. A system was designed to gather hardness data via flat punch indentation of cryocooler formed solidified nitrogen samples. The system was used to collect data at temperatures between 30 and 40K at 1-degree increments. Hardness averages ranged from 0.35 Mpa to 2.26 Mpa as temperature decreased, the data were approximately 3 to 4 times harder than prior data. The system was modified and used to conduct rotary shear testing. Based on the results, suggestions for further work are provided.

Acknowledgements

The path to finishing this thesis and project has occurred over the course of many years predating the project itself. I would like foremost to thank my advisor Dr. Mike Maughan, who has been both teacher and mentor. I've had the pleasure of learning from and working with Dr. Maughan since the sophomore year of my undergrad degree before the opportunity for this project arose. He encouraged me toward my potential and helped me further see how much I enjoy working on the research and development side of things. Dr. Jacob Leachman and the team over at the WSU HYPER Lab also have my deepest gratitude, this project would not have been feasible without use of their cryogenic test equipment and knowhow. Starting from the ground floor and knowing nearly nothing of cryogenics I was able to learn everything needed from them as well as rely on their expertise in areas that I had yet to learn. The project was funded through NASAs Glenn Research Center, under grant number 80NSSC19K0250. The team at Glenn was great to work with and always eager for results. Of note out of the team is Dr. Jason Hartwig, who I interned under at NASA Glenn after the lab portion of the project was completed. Dr. Hartwig's guidance and mentorship have helped shape the path of my professional career though the extensive variety of projects I was able to work on during my time at NASA Glenn.

Dedication

My biggest thanks go out to my parents John and Priscilla, who have been a large source of encouragement throughout this journey. They saw my leanings towards engineering from an early age and provided support through everything. I would also like the thank my Fiancée Randi for her continual support in writing this thesis. Having already completed her master's the support through the minutia, as well as a second set of eyes throughout the process have been invaluable.

Table of Contents

Abstract ii

Acknowledgements iii

Dedication iv

Table of Contents v

List of Figures vii

Chapter 1: Introduction 1

Chapter 2: Background 2

2.1 Literature Review of Existing Solid Nitrogen Data 2

2.2 Triton Terms 3

2.3 Cryogenics Terms 3

2.4 Indentation Terms 5

Chapter 3: Equipment Design 6

3.1 Cryostat Tester 6

3.2 Hardness Test Apparatus 10

3.3 Rotary Tester 14

3.4 Equipment Validation 17

3.5 Rotary Validation 18

Chapter 4: Experimental Methods 19

4.1 Sample Creation Process 19

4.2 Indentation 20

4.3 Rotary 21

4.4 Dry Ice Comparison 22

4.5 Data Processing 22

Chapter 5: Results 24

5.1 Indentation 24

5.2 Rotary 32
Chapter 6: Discussion 34
Chapter 7: Conclusion 37
References 38
Appendix A - Equipment List 40
Appendix B - Additional Dry Ice Data and Spring Validation Plots 41
Appendix C - MATLAB Processing Example Code 45
Appendix D - Arduino Example Code 57

List of Figures

Figure 2.1. System heat flow. 5
Figure 3.1. O-ring groove and two bolt holes 6
Figure 3.2. Top view of cryostat prior to modification. 7
Figure 3.3. Cryostat Interior. 8
Figure 3.4. Lake Shore Cryotronics 336 Temperature Controller. 9
Figure 3.5. Electronics system block diagram. 11
Figure 3.6. Indentation tester layout. 12
Figure 3.7. Rotary scraping tester block diagram. 15
Figure 3.8. Rotary test apparatus. 15
Figure 3.9. Rotary scraper dynamometer head. 16
Figure 3.10. Relevant dimensions of the scraping blades. 16
Figure 3.11. Control setup. 17
Figure 3.12. Instrumented indenter force vs. displacement data with overlaid spring constant line. 18
Figure 4.1. Indenter collecting data on dry ice. 22
Figure 4.2 Visual representation of data processing. 23
Figure 5.1. Hacker vs. Trepp data plot, multiple indenter diameters (mm) shown. 24
Figure 5.2. Data Averages. 25
Figure 5.3. Representative runs from 31 K to 39 K. 26
Figure 5.4 Indenter data at 31 K at positions 2 and 3. 27
Figure 5.5 Indenter data at 32 K. 27
Figure 5.6 Indenter data at 33 K. 28
Figure 5.7 Indenter data at 35 K. 29
Figure 5.8 Indenter data at 36 K. 29
Figure 5.9 Indenter data at 37 K, note two indenter sizes used. 30
Figure 5.10 Indenter data at 38 K. 30
Figure 5.11 Indenter data at 39 K. 31
Figure 5.12 Uncorrected full cycle runs at 39 K. 32
Figure 5.13 Rotary data. 33
Figure B.1. Combined Average of all Dry Ice Runs. 41
Figure B.2. All Dry Ice Runs 41
Figure B.3. Spring Three, Hillman 540058 for Verification. 42

Figure B.4. Spring Two, Hillman 540084 for Verification. 43
Figure B.5. Spring Four, Hillman 540045 for Verification. 43
Figure B.6. Spring One, Hillman 540464 for Verification. 44

Chapter 1: Introduction

NASA's interest in exploration extends to all areas within our solar system, including exploration of outer solar system bodies. This thesis is derived from a proposed NASA project, Triton Hopper, which is a probe concept under the NASA Institute for Advanced Concepts (NIAC). The proposed probe would land on Triton, a moon of Neptune, whose surface is primarily solid nitrogen (SN_2), to perform observation and surface sampling. It is anticipated that the probe will use nitrogen (N_2) gathered on site for flight over the moon's surface. One proposed method is to mechanically gather SN_2 from Triton's surface, which would then be heated and gasified, greatly expanding the volume. The gas would then be expelled through a nozzle to provide flight to the vehicle, allowing it to "hop" between locations on Triton's surface. The desire to explore Triton stems from its status as a captured Keiper belt object, as well as its similarities to Pluto, while being much closer to Earth and thus a shorter flight time.

This study gathered data to inform the design of a physical apparatus for collection of solid nitrogen. A custom test apparatus was developed to obtain solid nitrogen hardness data, which replicated Triton's surface conditions. Commercial equipment for testing of solid cryogens does not exist thus a customized solution was necessary. To meet requirements a generalized indentation apparatus was heavily modified to allow mounting of both indentation and shear testing apparatuses.

Chapter 2: Background

2.1 Literature Review of Existing Solid Nitrogen Data

There is sparse existing hardness data available in the appropriate temperature and pressure domain of Triton's surface. Hartwig and Sagmiller, [1] completed an extensive literature review of N_2 properties. This author also completed a literature search and came to the same conclusion regarding the availability of published mechanical testing of solid nitrogen results in the same temperature range.

Only one source of hardness data was found, Trepp [2]. Trepp reported indentation hardness using a stainless steel 90º conical indenter. Regarding stress-strain data, only two sources were found. Leonteva et al. [3] conducted tensile testing on a variety of noble gas cryocrystals using a unique testing apparatus, and more recently, Yamashita et al. [4] conducted unconfined compression tests on 10 mm diameter cylinders of SN_2. For landing on and proposed mechanical collection mechanisms of SN_2 on Triton missions, confined compressive hardness is a critical metric for engineering design. While the above data was informative, mission planners for Triton Hopper desired more focused testing of SN_2 at the expected surface conditions. As a point of comparison NASA ran two robotic mission sets in the 1960's Ranger [5], and Surveyor [6], to gather surface data on the moon prior to the Apollo missions to help determine if the planned moon landings were feasible. The Ranger program took photos of the moon's surface as each craft approached and subsequently crashed into the surface. The Surveyor craft subsequently landed on the moon's surface to take close up imagery and mechanically sample the soil. Both programs operated at significant financial cost, notwithstanding the failure of eight out of sixteen craft. For the Triton Hopper mission, being able to gather requisite surface property data in the lab represents a significant cost savings compared to sending a separate test probe.

2.2 Triton Terms

2.2.1. Triton

2.2.2. Triton is a moon of Neptune whose surface pressure is estimated to be 1.6 Pa [7], and has a surface temperature between 30 K and 40 K [8]–[11]. Triton has a diameter of roughly 2700 km [12] and is thought to be a captured Kuiper belt object [13]. This is relevant as Pluto is also thought to be a Kuiper Belt object. Information gathered on Triton could be used to further the understanding of Pluto and the Kuiper belt in general. Pluto is located an average of 39 AU's [14] from the Sun, Neptune around which Triton orbits is only 30 AU's [15] from the Sun. This difference in distance from the Sun, and correspondingly Earth, combined with a double gravity assist allows for a 12 year transit time [13] between launch from Earth and landing on Triton. The shorter distance from Earth to Triton as compared to Pluto also reduces communication delay and increases data rates. These and other reasons make Triton an object of object of interest for landing on as opposed to Pluto. Triton Hopper

Triton Hopper is a proposed space vehicle for which this research was funded. The concept is to send a research probe to the surface of Triton. To maximize scientific potential of the mission, access to many geographical regions is desired. Flying sufficient propellant from Earth to complete the mission would not be feasible so other options were explored. Two similar proposals, both using in situ gathered nitrogen were determined to be the best solutions. One proposal is to pump nitrogen from the atmosphere, solidifying it within the craft for later use. The second proposal, and more relevant to this research, is to mechanically gather solid nitrogen from the surface. The gathered nitrogen would then be heated from solid to gas by a radioisotope thermoelectric generator. This high-pressure gas would then be used as a propellant with a nozzle to provide propulsion, allowing the craft to relocate.

2.3 Cryogenics Terms

The science of Cryogenics is that which looks at the production and effects of very low temperatures. Temperatures below 120 K are considered cryogenic [16] as at and below 120 K many pure gasses liquefy. Cryogenic work accelerated in the mid to late 1800's as many purified gases were liquefied in succession.

2.3.1. Vacuum Systems

The majority of cryogenic test systems require a vacuum system. With high temperature differences between the atmospheric environment and cryogenic test articles, convective heat transfer becomes significant. To reduce the energy input, a high vacuum system is typically used to remove the majority of the atmosphere from the chamber, taking the remaining atmosphere in the system

from the standard flow regime into the molecular flow regime. This greatly reduces convective heat transfer. The hardware is typically comprised of a standard vacuum pump backing a turbo molecular pump. The combination can achieve a high to ultra-high vacuum. The standard vacuum pump reduces system pressure from atmospheric to the $1x10^{-2}$ mTorr range. Once stabilized, the turbo molecular pump is enabled which further reduces system pressure to $1x10^{-5}$ mTorr and below. This takes the system into the molecular flow regime thus effectively eliminating convective heat transfer.

2.3.2. Multi Layered Insulation (MLI)

MLI is used in the vacuum chamber to reduce radiant heat transfer between the chamber walls and the experiment. Since radiant heat transfer scales with the fourth power of temperature differential (ΔT^4) it becomes the dominate transfer mechanism for large temperature differentials. MLI is typically comprised of a metalized film [17] and a low conduction separation material (often fiberglass) in repeating layers.

2.3.3. Cryocoolers

Cryocoolers are a class of coolers that can achieve cryogenic temperatures. The main varieties are Stirling, Gifford-McMahon, and pulse tubes. Efficiency levels vary, though none of the coolers are particularly efficient due to the nature of pumping heat across the extreme temperature differentials found in cryogenic systems. The CRYOMECH PT405 cryocooler used in this research is a pulse tube which relies on oscillation thermodynamics [16].

2.3.4. Thermal Dead End

A thermal dead end is a specific type of location within a heat transfer system where temperature will reach equilibrium. The thermal dead end will come to temperature equilibrium at the junction of the heat flow leads (see Figure 2.1). This is caused by the definition of heat, that being, the energy flow along a temperature gradient. With the dead end being at the same place along the gradient it will come to rest at the same temperature. There will be thermal lag due to mass, but temperature will equilibrate across the area.

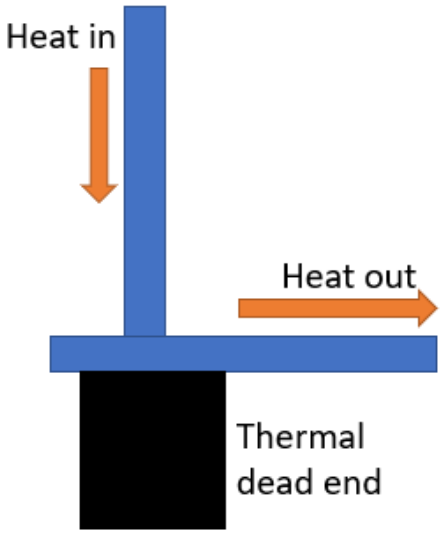

Figure 2.1. System heat flow.

2.3.5. Cryostat

Cryostat is a general term for a cryogenic testing apparatus. Various types of cryocoolers or cryogenic liquids can be used for cooling. Cryostats often use vacuum systems and MLI to minimize heat into the cryogenically cooled portion of systems.

2.4 Indentation Terms

Indentation testing is a common type of test that can provide hardness and elastic modulus information depending on the specific test. Hardness is roughly defined as a material's resistance to permanent indentation [18]. Indentation tests range from older standards such as the Brinell or Rockwell Tests to more recent nanoindentation techniques. Many indentation techniques require post-indent inspection to determine indent area. Alternatively contact area is a function of depth and can be used to calculate hardness if the probe is calibrated in a known material and the instrument provides indentation depth.

2.4.1. Flat Punch

The exception to general indentation is flat punch indentation, which uses an indenter that has constant area with varying depth. The advantage of this is that no post indent visual inspection is needed to determine indent area and thus sample hardness. Flat punch indentation also simplifies the hardness equation to $H = \frac{P}{A}$ [19] where H is hardness, P is the maximum indentation force, and A is the cross-sectional area of the indenter.

Chapter 3: Equipment Design

3.1 Cryostat Tester

The test apparatus was integrated into an existing cryostat which was designed and built by researchers at the Washington State University's (WSU) Hydrogen Properties for Energy Research (HYPER) lab. The cryostat was originally built to test dissolved gases within cryogenic liquids [20], thereby supporting the early development of a Titan submarine. The cryostat used a 0.48 m x 0.57 m x 0.28 m stainless steel vacuum chamber as an enclosure which was supported externally, off the ground, by an extruded aluminum frame. The chamber had five penetration locations. Primary access was through the front of the chamber where a large rectangular opening with rounded edges was cut through the face. The opening left roughly 10 cm of material between the cut and chamber edge. This material provided space for sealing and attachment of the face plate. About one cm from the inner edge, an O-ring groove was cut into the panel face, (see Figure 3.1). Slightly out from the groove, eight tapped blind holes were cut into the face for bolting on the cover plate. Beyond these, four additional blind tapped holes, one at each corner, were used to bolt short pieces of threaded rod. The rods allowed for temporary hanging of the cover plate while it was bolted into place.

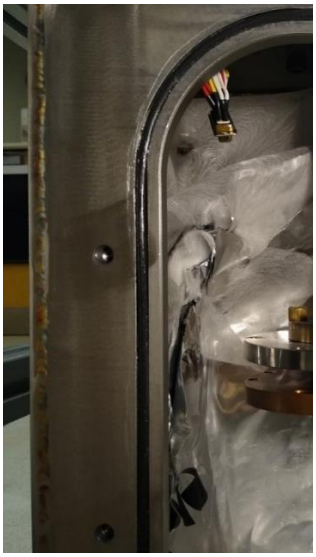

Figure 3.1. O-ring groove and two bolt holes.

Three of the five penetrations were located on the top of the chamber. One each for the cryocooler, sensors, and experiment. The cryocooler was a Cryomech PT405 pulse-tube used in conjunction with a Cryomech Cold Helium Circulation System. Heat generated by the cryocooler was rejected to a building water loop through a pump and liquid-to-liquid heat exchanger. Access to

internal sensors was provided by a welded VF flange on the top of the chamber (see Figure 3.2). A four-way adaptor was bolted to the flange to provide three access ports. Internal wiring for sensors and heaters was run through one port, a vacuum sensor was attached to the second port. The third port was used to refill the chamber to atmospheric pressure after tests were completed. The third hole though the top of the chamber provided access to the experiment. As with the front panel cutout, an O-ring groove was cut into the plate, surrounding the groove six blind tapped holes provided mounting. The final penetration was located on the back of the chamber and was used to connect the vacuum system. The vacuum system used a Leybold DB8 rotary vain vacuum pump in series with an Agilent Tv 81m turbomolecular pump. This combination provided a typical 10^{-5} to 10^{-6} mtorr vacuum at room temperature, and cryopumping dropped this an additional order of magnitude during operation.

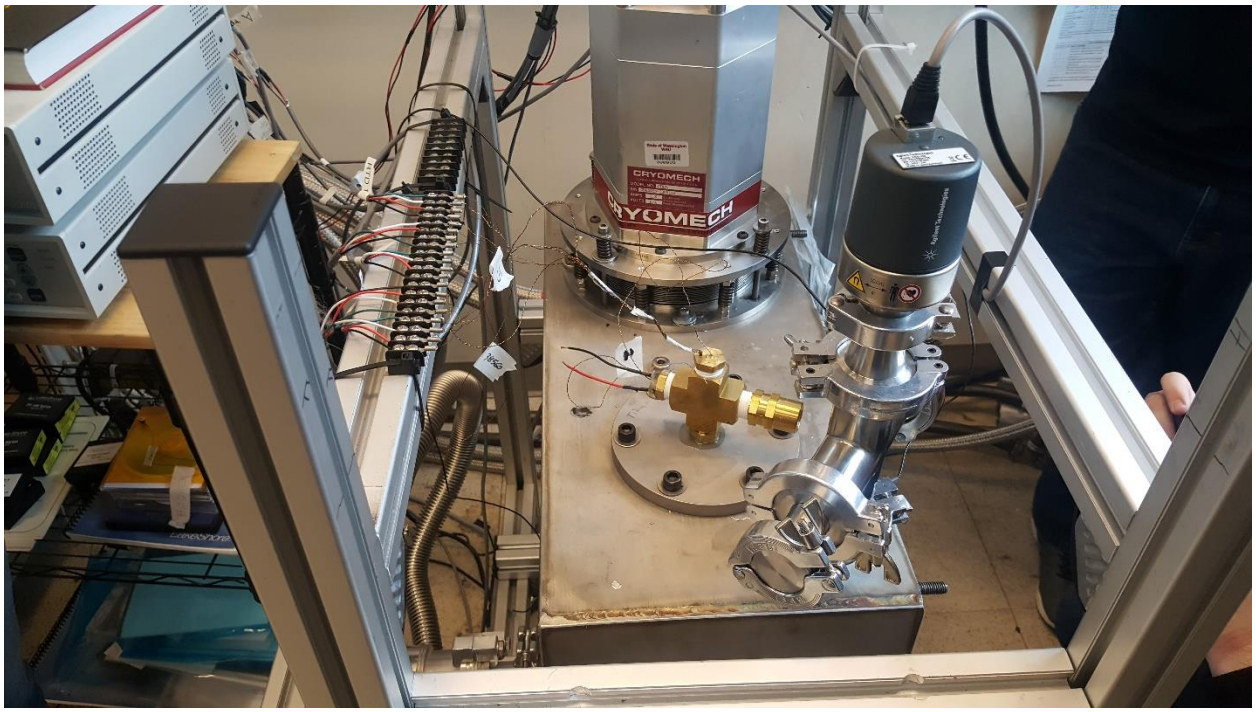

Figure 3.2. Top view of cryostat prior to modification.

Inside the cryostat, a heat break and busbar help to cool and mount the experiment. Figure 3.3 shows the heat break which provides mechanical mounting of the test cell to the vacuum chamber and direct access to the sample. The top of the heat break is sealed to the bottom of the experimental

passthrough hole. The busbar uses a 12.7 mm thick copper bar that thermally links the second stage of the cryocooler to the experiment, (see Figure 3.3).

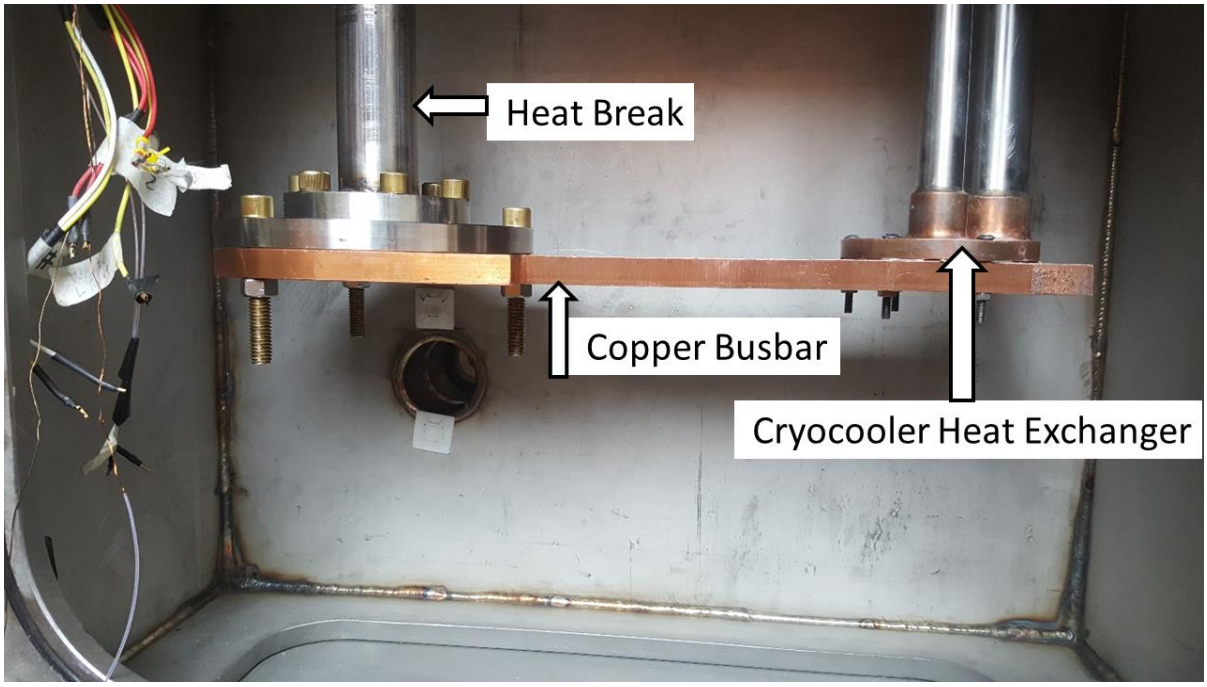

Figure 3.3. Cryostat Interior.

3.1.1. Cryostat temperature control system

To maintain a constant temperature, cryocooler based systems need a temperature controller. The cryocooler itself is not throttleable and thus removes heat based on its performance curve. To maintain a set temperature a controlled heat input is required to counteract the cryocooler. To accomplish this a Lake Shore Cryotronics 336 (336) temperature controller shown in Figure 3.4 was used. The 336 has four independent temperature sensor input/outputs that can be used with diode, resistance temperature detector (RTD), and thermocouple type sensors. An in-house calibrated RTD from Lakeshore Cryotronics was connected to one of these ports. The 336 has multiple direct heater outputs and connections for use with external amplifiers. Outputs are mapped to sensor inputs in the settings menu. Output is determined by a maximum output power limit, with a percentage of that being set by either a PID control loop or manual override. The PID values can be set either manually or via an automatic tuning routine. The system autotuning was unsuccessful so values were set manually.

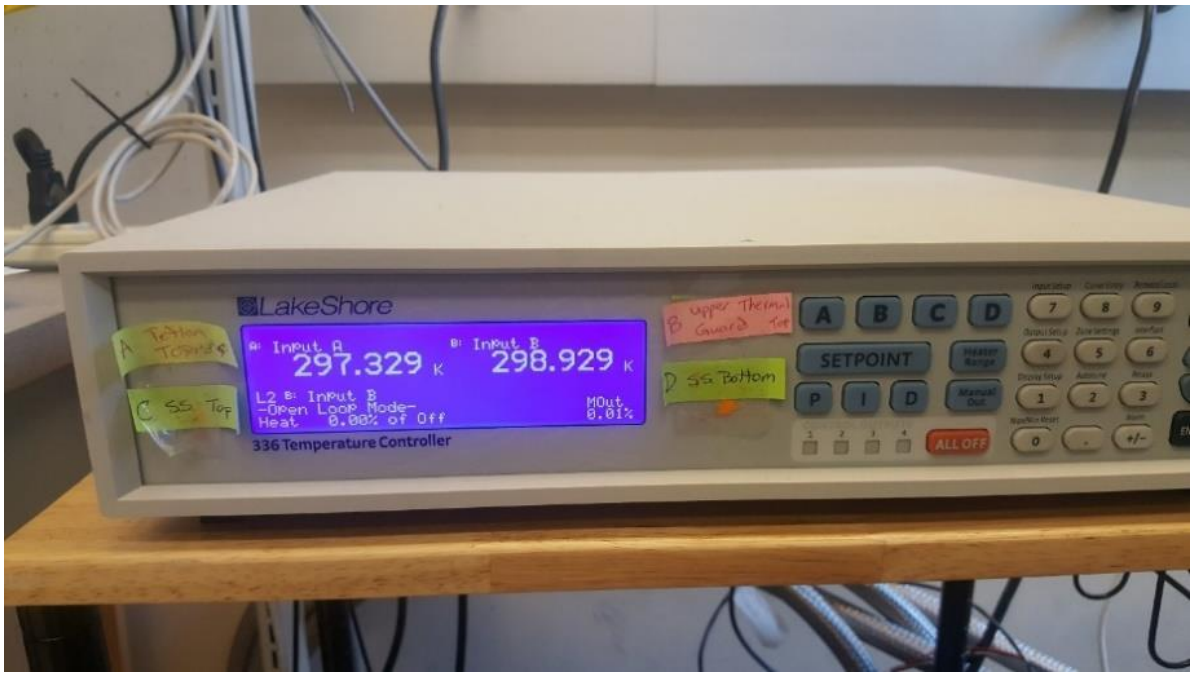

Figure 3.4. Lake Shore Cryotronics 336 Temperature Controller.

A germanium RTD sensor was attached on the bottom exterior of the sample cup was used to provide the primary temperature reading. A resistance heater wrapped around the side of the sample cup was also connected to the 336 and tied to the germanium RTD. This combination allowed fixed temperatures to be set with the cryocooler running. It was also used to expedite warming of the system to either melt the sample or to bring all internal material up to room temperature so the chamber could be opened when modifications to the system were needed.

3.1.2. Material Choice

Material choices in cryogenic systems are key due to the wide temperature range over which they must operate. Depending on location, low or high thermal conductivity is required for best performance. Parts that extend from the cold stage of the test apparatus to hot regions, typically room temperature, need low thermal conductivity. This minimizes heat transfer, but the material must also balance thermal conductivity against the required mechanical strength and durability needs.

For low heat transfer parts, titanium grades 5 and 9, Ti-6AL-4V and Ti-3AL-2.5V respectively, as well as 316 stainless steel were used. These materials have low thermal conductivity while maintaining reasonable machinability. In this apparatus the thermal break, which mechanically

mounts the test apparatus in the cryostat, is 203 mm in length with a 260 K temperature differential during operation. Stainless 316 was used because it allowed machining and reuse of mounting flanges from an existing heat break. A new 38.1 mm diameter, 0.89 mm wall, stainless 316 tube was welded in providing excess diametral room for the indentation shaft while not exceeding the O-ring inner diameter at the top of the chamber where it was bolted to the vacuum chamber. The 0.89 mm wall thickness was chosen due to availability, as it was the thinnest wall easily available. The shaft between the load cell and indenter assembly was intended to be Titanium 6Al-4V, grade 5. Procuring Ti 6AL-4V in the 28.6 mm diameter thin wall tube was not possible, so grade 9 tubing with a wall of 0.71 mm was substituted. The grade 9 tube was welded to grade 5 plugs located on each end to provide sealing and mounting for the needed hardware.

Indium was used in metal-to-metal seals to maintain airtightness between the thermal break, busbar, and sample cup. Indium wire was formed into rings and placed in machined grooves on the top of the busbar and sample cup. When the joints were bolted together, the compression deformed the indium creating the seal. Other metals such as copper are also used in metal-to-metal seals but are typically supplied pre-formed for use with specific connectors and do not provide the installation flexibility of indium necessary for custom applications such as this test. Polymeric materials like butyl O-rings harden at cryogenic temperatures and have varying thermal expansion rates which make them unsuitable for these locations.

3.2 Hardness Test Apparatus

3.2.1. Control System

To control the tester and gather data, a control system had to be developed. The ideal system had low input/output signal requirements and no need of real time data processing. A custom solution was determined to be the best option. Off-the-shelf sensors, amplifiers, and motor drivers were purchased and connected to a computer via Arduino Mini microcontrollers. A schematic of the system components is shown in Figure 3.5.

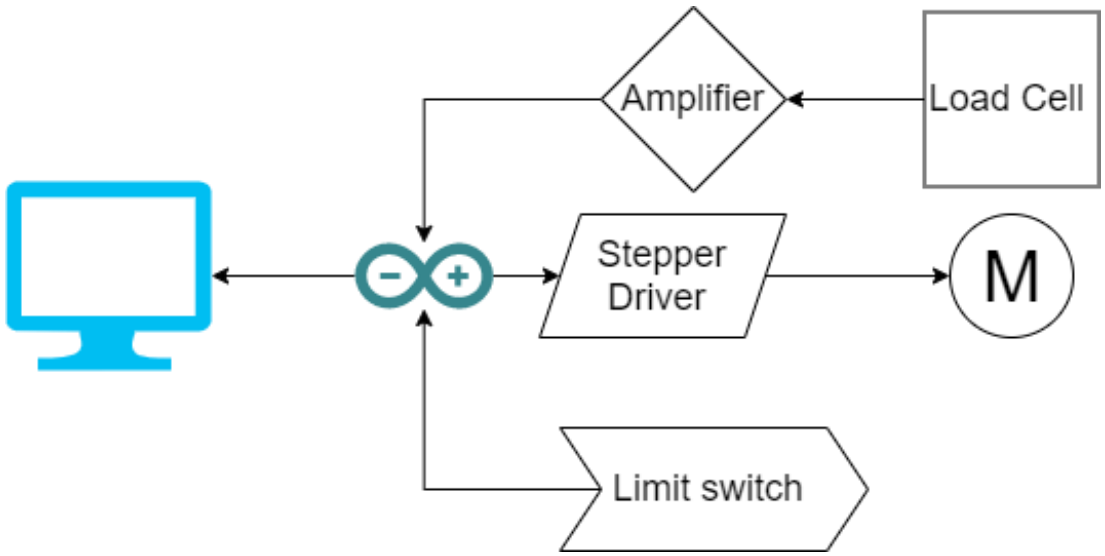

Figure 3.5. Electronics system block diagram.

Arduino code was written to input the sensor data and output calibrated force and displacement data to an attached PC through serial communication over USB. This output was monitored and stored in text files (.txt) for later processing. These files stored system time, displacement from limit switch in millimeters, and force in grams. Data were processed via MATLAB scripts. For ease of assembly and initial troubleshooting, the Arduino, load cell amplifier, and motor driver were installed in a breadboard. Once verified, the first iteration was left in the breadboard for testing.

A NEMA 17 motor and A4988 stepper driver were used to validate system movement. Higher than expected drive resistance was encountered which came from two sources. The first was from the load frame drive threading. When the load frame was tightly bolted to the cryostat some binding occurred. This was remedied by tightening in a cross pattern and decreasing to a finger-tight torque. Secondly, and the more serious of the two, additional resistance was due to O-ring drag. Even with Dow Corning high-vacuum grease applied to reduce friction the NEMA 17 could not provide sufficient torque, so the motor was changed to a NEMA 23 using an off-the-shelf stepper driver with sufficient power.

3.2.2. Mechanical Design

It was determined in the early stages of mechanical concept development that a custom indentation tester would be needed to meet the project goals. Initially a fully custom linear motion setup was considered, however due to time constraints it was determined that this would not be

feasible. The final tester utilized a combination of off-the-shelf hardware and custom-made components. A MARK-10 ES20 load frame was purchased with the intent of modification. The load frame is rated for 500 N and had sufficient travel. The ES20 was disassembled for machining of the base plate. A central experimental passthrough and holes for the six mounting bolts were added. Separately an O-ring sealing block was manufactured. The block sealed the indenter shaft and provided a port for adding and removing N_2 gas from the test chamber. To seal the shaft, two O-rings were used. The O-ring geometry was designed to recommended specifications in the Parker Hannifin O-ring Handbook [21] for a high vacuum system with linear actuation. A mounting bracket was made to mount the load cell under the cross-head as the shaft center had been moved back relative to the intended application. To mount the drive stepper motor in place of the stock rotary handle a mount was fabricated via 3D printing. A diagram showing the layout of the previously described components is shown below in Figure 3.6.

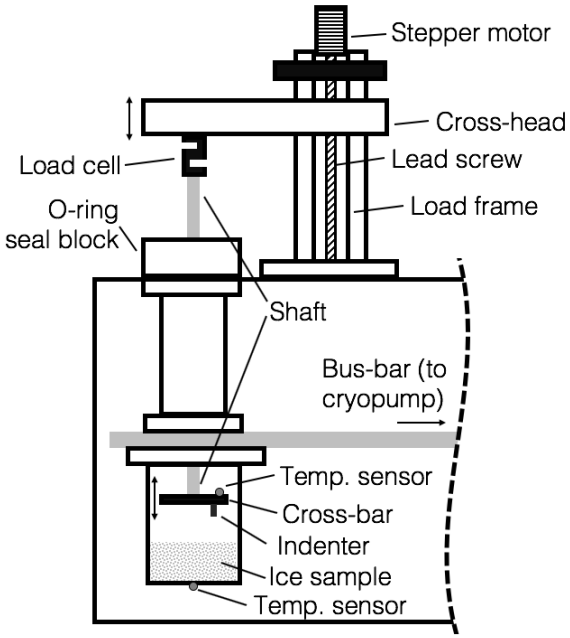

Figure 3.6. Indentation tester layout.

3.2.3. Indentation Tester

Trepp's [2] work was used for initial load estimation. Considering the geometrical differences between conical and flat-punch indenters there was some uncertainty in the expected deformation pressure. If the force was not within an acceptable range, the flat-punch indenter could be easily changed out for a different size. Initial testing found that an indenter sufficiently sized to give a good

reading at 36-39 K overloaded the load cell at 31-34 K due to the temperature-dependent nature of nitrogen's hardness, so indenters of 2.25 mm, 2.77 mm, and 4.11 mm in diameter were used depending on temperature. For ease of manufacture and cost effectiveness ¼-20 Ti-64 bolts were modified on a lathe to a flat punch geometry on one end while maintaining the threading on the other. This allowed easy changing of the indenter when the test chamber was opened.

3.2.4. O-ring Drag Measurement and Data Correction

During the design process calculations were made to estimate the O-ring drag force to determine if the drag force would be negligible or something that would factor into the design. Formulas from the Parker Hannifin O-ring Handbook [21] sections 5.11-5.14 were used. Assumptions were for two O-rings with 5% compression and a 70-shore durometer hardness to maintain 70 kPa of sealing. This resulted in a 29 N drag estimation; even with a safety factor of three the drag force would be well within acceptable limits.

To achieve a smooth surface finish for sealing, the titanium shaft was wet sanded with successively finer sandpaper from 600 grit to 2000 grit. During initial installation, no lubricant was applied between the titanium shaft and O-rings, which resulted in a frictional force estimated at above 220 N. To reduce friction, Dow Corning high-vacuum grease was applied to the O-rings, O-ring block, and a thin film was applied to the titanium shaft. After assembly of the apparatus was completed the apparatus was repeatedly cycled to confirmed operability.

3.2.5. Electronics

To obtain a force reading an S-beam load cell was installed into the system. To connect the load cell into the Arduino an HX711 breakout board was used to amplify and read the signal. A limit switch to provide positional zeroing was directly connected to the Arduino. Indentation displacement was instead calculated using the pitch of the lead screw in the load frame, steps per revolution of the stepper motor, and counting the number of step signals sent to the stepper driver from the Arduino. Travel was validated using calipers after each system or code change. The TMC5160 SilentStepStick motor drivers were selected to drive the motors. The TMC5160 can provide a drive current of 3A RMS (4.2A peak) at a maximum of 60 volts. This allowed near full torque from the selected NEMA 23 stepper motors which had a rated operational current of 4.2A.

3.3 Rotary Tester

3.3.1. Rotary Mechanism Design

It is reasonable to conceive that mechanical gathering of SN_2 could be accomplished via a rotary mechanism. Ice core drilling is an example of such a mechanism that could be employed on the Triton Hopper. To help understand the mechanics of such a process, a rotary tester to measure vertical force and torque requirements was developed, simulating a drilling mechanism in Triton-relevant conditions. The design utilized the basic framework of the previously described indentation tester.

The design used rod-end bearing joints and a 12 mm linear rod to constrain motion such that the two load cells measured independent forces. The design required shortening of the load frame arm to allow for the additional hardware at centerline. The rotary motion was provided by an off-the-shelf NEMA 23 stepper motor with a torque rating of 3 N-m. This was the same model motor that was used to drive the lead screw on the load frame.

The rotary scraping device was adapted to the load frame and cryostat previously described and is shown schematically in Figure 3.7, and photographically in Figure 3.8. The device contains a dynamometer to measure torque while the rotating tool attachment is driven into the SN_2 sample. The dynamometer functions by transferring all rotational forces through a horizontally oriented load cell. The stepper motor rotating the shaft is secured to the base plate. The base plate pivots around and translates on the pivot rod. Rotational torque is calculated based on the horizontal load cell force measurement. The load cells are mounted on spherical bearings at both ends. The vertical load cell connects the bracket mounted on the backing plate to the base plate. The pivot rod is mounted rigidly to the backing plate. The shaft passes through a hole in the base plate before entering the O-ring seal and specimen chamber. The backing plate is mounted rigidly to the cross-head so that the shaft connected to the assembly and blades can be driven into the ice surface. Initial installation with a solid coupler resulted in oscillatory force readings indicating the alignment was perfect. Changing the solid coupler to a flex coupler sufficiently damped off-axis motion detected by the torque load cell.

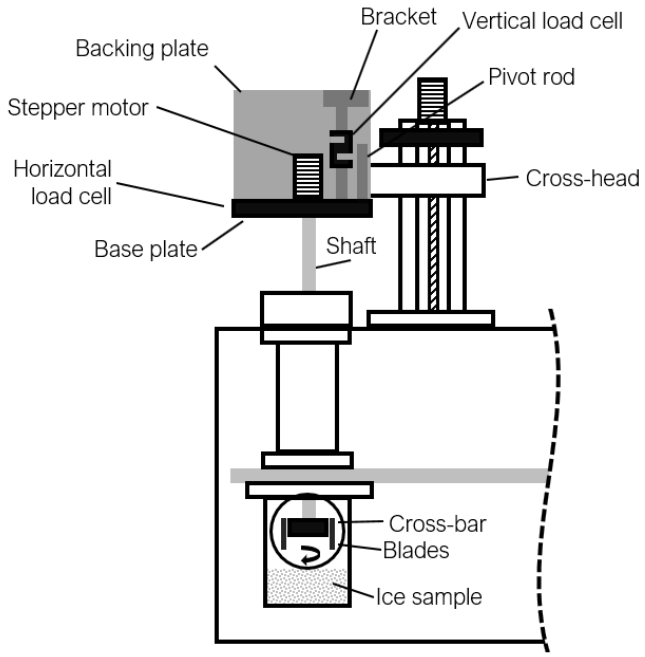

Figure 3.7. Rotary scraping tester block diagram.

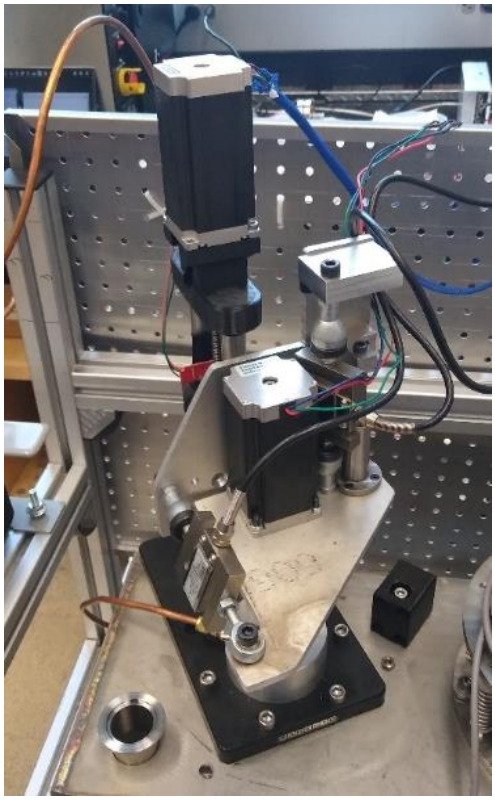

Figure 3.8. Rotary test apparatus.

The rotary scraping head is comprised of an aluminum cross-bar with stainless steel blades attached by socket head cap screws. The blades have a thickness of 3.1 mm, a vertical scraping surface of 10 mm in height and a 5° relief angle behind the scraping point. The trailing edges were filed down to reduce possible interference between the SN_2 and non-cutting edge. A photograph of the cutting head is shown below in Figure 3.9. Other relevant dimensions of the scraping blades are shown below in Figure 3.10. The two blades had a 41.2 mm center to center distance.

Figure 3.9. Rotary scraper dynamometer head.

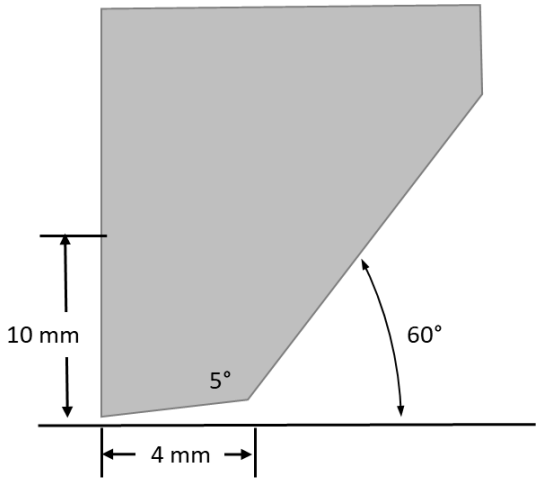

Figure 3.10. Relevant dimensions of the scraping blades.

3.3.2. Control System Updates

The control system was modified from the iteration seen in section 3.2 to facilitate rotation testing. The additional load cell and motor required adding additional modules to read and drive the items. A protoboard was built up to mount both stepper drivers and HX711 modules which solved the space limitations of the existing breadboard, shown in Figure 3.11. The rework also simplified wiring and permitted easy mounting of a cooling fan to cool the modules. The TMC5160 drivers were mounted at this point.

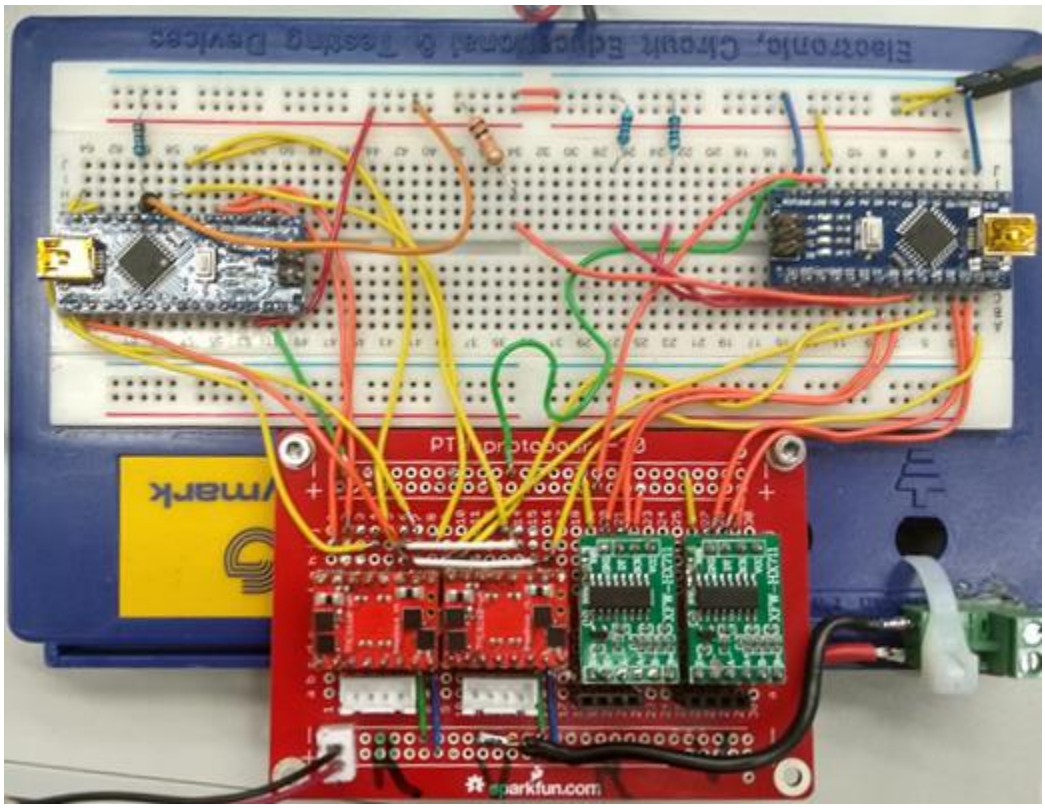

Figure 3.11. Control setup.

3.4 Equipment Validation

3.4.1. Spring Validation Testing

To validate that the indentation test system was delivering correct data, two spring-force validation tests were conducted using four different springs produced by the Hillman Group. Force vs. displacement data were collected from each spring with the system open and at room temperature. The four springs have constants of 0.129 kg/mm, 0.224 kg/mm, 0.278 kg/mm, and 1.17 kg/mm. The

data were corrected via the drag-force correction procedure described in Section 3.3. A very good fit to the known constant was achieved with all four test springs through multiple runs. The force vs. displacement data were plotted against spring four's force-displacement in Figure 3.12. Additional spring plots are located in the appendices. The results were consistent with expected values for all springs across all test trials. Test results indicated appropriate system compliance and calibration.

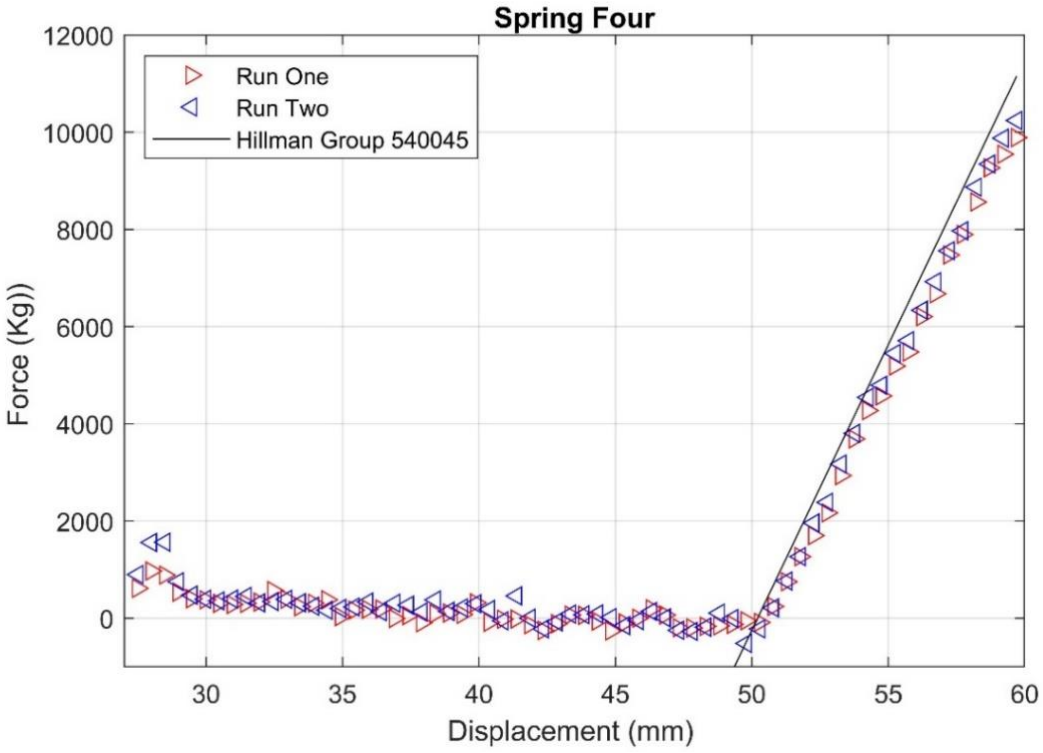

Figure 3.12. Instrumented indenter force vs. displacement data with overlaid spring constant line.

3.5 Rotary Validation

The load cell used for torque measurements was given a multi-point calibration against a known scale to validate the rotary head torque readings. Using the force reading and known distances, the force couple was used to calculate torque.

Chapter 4: Experimental Methods

4.1 Sample Creation Process

The following section describes what steps were taken to ensure consistent experimental results.

During each resealing of the cryostat and internal test cell, care was taken to ensure proper sealing of all components. For metal-to-metal seals, any remaining indium from previous seals were carefully removed. Mating surfaces were cleaned with a solvent, either 99% isopropyl alcohol or methyl ethyl ketone, prior to new indium wire being applied. A similar approach was taken with the main O-ring seal on the chamber and its associated sealing surfaces. The door sealing surface was cleaned with solvent each time, and the O-ring was wiped down with Kimwipes to remove any contaminates. If contaminates remained, such as glass fibers from the MLI, the O-ring was removed for cleaning and the groove in the chamber was cleaned as well. While small, any glass fibers bridging across the O-ring could cause a leak despite the application of Dow Corning high-vacuum grease on the mating surfaces.

With the internal test cell sealed, a vacuum pump was used to remove air from that subsection. Once a pressure of $1x10^{-3}$ mbar was reached the valves were closed and vacuum pump shut off leaving a closed subsystem. During initial testing this was left overnight, with a vacuum gauge being checked before and after to determine if the test cell was properly sealed. In later test stages this wait time was reduced to one hour. With the seal verified, 99.999% pure N_2 gas was used to purge the system of gaseous contamination. To do this, the test chamber was filled with N_2 gas to about 70 kPa, the gas inlet valve was then closed. With the vacuum pump running and outlet lines already evacuated, the outlet valve was slowly opened allowing the pump to pull a vacuum on the test chamber. The outlet valve was closed, inlet valve opened, and the test chamber was refilled with N_2 to about 70 kPa. This process was repeated three times until the third N_2 fill was purged.

Next, the door plate was bolted to the cryostat and vacuum system was used to pump down the cryostat chamber. As mentioned in Chapter 2, vacuum pumping used a two-stage process because a single-stage pump would not provide enough vacuum to allow the cryostat to reach the required temperatures. A Leybold DB8 rotary vain vacuum pump was applied until the pressures reached the 10^{-3} mbar range. If the pressure did not drop, the door was tightened. If this step was unsuccessful, the door was then removed to check for leaks, and then resealed. When properly sealed, the time to sufficient pressure drop took between 20 and 40 minutes. Once stable, an Agilent TV81M

turbomolecular pump was turned on to further reduce chamber pressure to the 10^{-5} to 10^{-6} mbar range. The cryocooler was then turned on and the apparatus left for 18-24 hours. During this time, heat was conducted away allowing the copper busbar and test cup to reach equilibrium temperature, which varied between 28 K and 30.5 K.

With the test cell at steady state temperature, the gas system was used to fill a small tank of known internal volume. The fill valve from the main tank to the smaller tank was then turned off and the pressure in the small tank recorded. Another valve between the small tank and system was then opened allowing gas to flow into the sample cup. Due to the thermal capacity of the busbar bar and sample cup, the entire charge of N_2 liquefied as soon as it entered the sample area. The valve was closed once the pressure stabilized and flow stopped. The pressure on the small tank was then recorded. This process was repeated a second time to achieve the desired sample thickness. Using the tank volume, temperature, and total pressure difference, the fill volume was calculated. Immediately after filling the system the sample cup was between 80 K and 85 K. After filling the cryocooler was left to run, bringing all components in the system to equilibrium temperature which again varied between 28 K and 30.5 K. Cooling from the low 80 K range to 30 K took between 6 and 8 hours with a constant rate. In cases where successive samples were run without need for mechanical changes to the system the sample was reset. This involved turning off the cryocooler and manually turning on the heater until the sample cup was between 70 and 80 K, which ensured the sample was completely reliquefied. The heater was then turned off and the cryocooler restarted. The cooling time was similar to a fresh sample. If the test temperature of the next run was known it was input to the Lakeshore 336 temperature controller, which would hold the desired temperature once reached.

4.2 Indentation

When the samples were stable at the desired test temperature for a minimum of 30 minutes, the indentation procedure could begin. Indentations were primarily performed in sets at a given test temperature. To begin the indentation, the tester was powered on and connected to a computer, the reset button on the Arduino Uno was then pressed to reset the program. This reset moved the indenter up until the limit switch was triggered, determining zero; the indenter then moved down 10 mm. The indentation tip was then manually plunged into rotary position 1 to cool, it was left for at least 30 minutes to stabilize temperature.

With temperature stabilized, the reset button on the Arduino was pressed again moving the device back to a 10 mm offset from the limit switch. The bolt holding the indenter shaft to the load

cell was loosened slightly, the indenter was rotated to position 2 and the bolt was retightened. The Arduino serial monitor on the computer was cleared and then the cycle button was pressed. This moved the indenter down to a preset displacement and then back up to the same offset. Force and position data were continuously sent to the Arduino serial monitor on the computer. With the run complete, auto scroll in the Arduino serial monitor was disabled and the contents copied into a text file. The naming scheme of each document indicates temperature and position of that run. The indenter shaft was then rotated to the next position and the process began again. All data generated in a day was saved to a folder with the test day's date.

4.3 Rotary

Rotary experiments were conducted in two modes, manual and motorized. With both setups, dynamic drag measurements were completed to zero the data in post-processing.

For manual measurements, once the sample was stable at temperature, the rotary head was lowered until it contacted the sample surface. This was done by pressing the down button while watching the vertical force reading, once the vertical force reading started to increase rapidly, indicating contact, the button was released. This was verified by trying to lightly rotate the shaft by hand, more resistance than expected for non-contact indicated that contact had been achieved. The rotary head was left in contact for approximately 30 minutes to cool before being rotated 360 degrees clockwise to ensure a flat surface. The apparatus was then lowered into the sample by either 2 mm or 3 mm depending on the run. Using a dial torque wrench, the shaft was then rotated by hand about 90 degrees in a period of approximately 20 seconds. A video recording of the torque wrench was made to record the data. The rotational position was then reset to its original position and lowered again by the same amount and the process was repeated two additional times such that three runs per sample creation were completed.

Mechanical rotary measurements were also completed using the apparatus described in section 3.3. Cooling the rotary device was completed in the same fashion as hand measurements. With the rotary head cooled, the head was raised to the starting position and rotary test program started. Rotation and plunge (penetration into specimen) were performed at constant rate. The plunge and rotation rates were 1 mm/revolution and 10 RPM respectively. The plunge rate was 10 mm/min which translates to a 0.5 mm depth of cut per blade with the two cutting faces on the head.

4.4 Dry Ice Comparison

The experimental processes were conducted on dry ice to provide a comparison for the SN_2 data. The same indentation procedure was followed with commercially sourced dry ice. Experiments were conducted at atmospheric pressure with an open test chamber. Suitably smooth blocks of dry ice were selected and placed under the indenter tip. Scrap aluminum was used to position the dry ice using the bottom of the cryostat chamber for support. The indenter probe was brought into contact with the specimen in rotary position 6 to achieve temperature equilibrium with the sample. The indentation procedure was then run for thirty indentations. The indents were physically spaced, and results recorded. Figure 4.1 shows a photograph of the indenter in contact with a block of dry ice.

Figure 4.1. Indenter collecting data on dry ice.

4.5 Data Processing

The drag noted in Section 3.2.3 varied with displacement during initial test runs. Further testing showed the drag to be a function of displacement that was consistent between runs in each rotational position. Data were recorded for two full displacement runs in each rotational position without a sample present. The data were then positionally averaged for each position giving a drag force vs. displacement curve. The drag curves were then subtracted via superposition from the sample

data. For plotting the data were then manually zeroed to account for slight differences in depth of impact and tared to give zero pressure prior to impact (zeroed). This process is visually represented in Figure 4.2

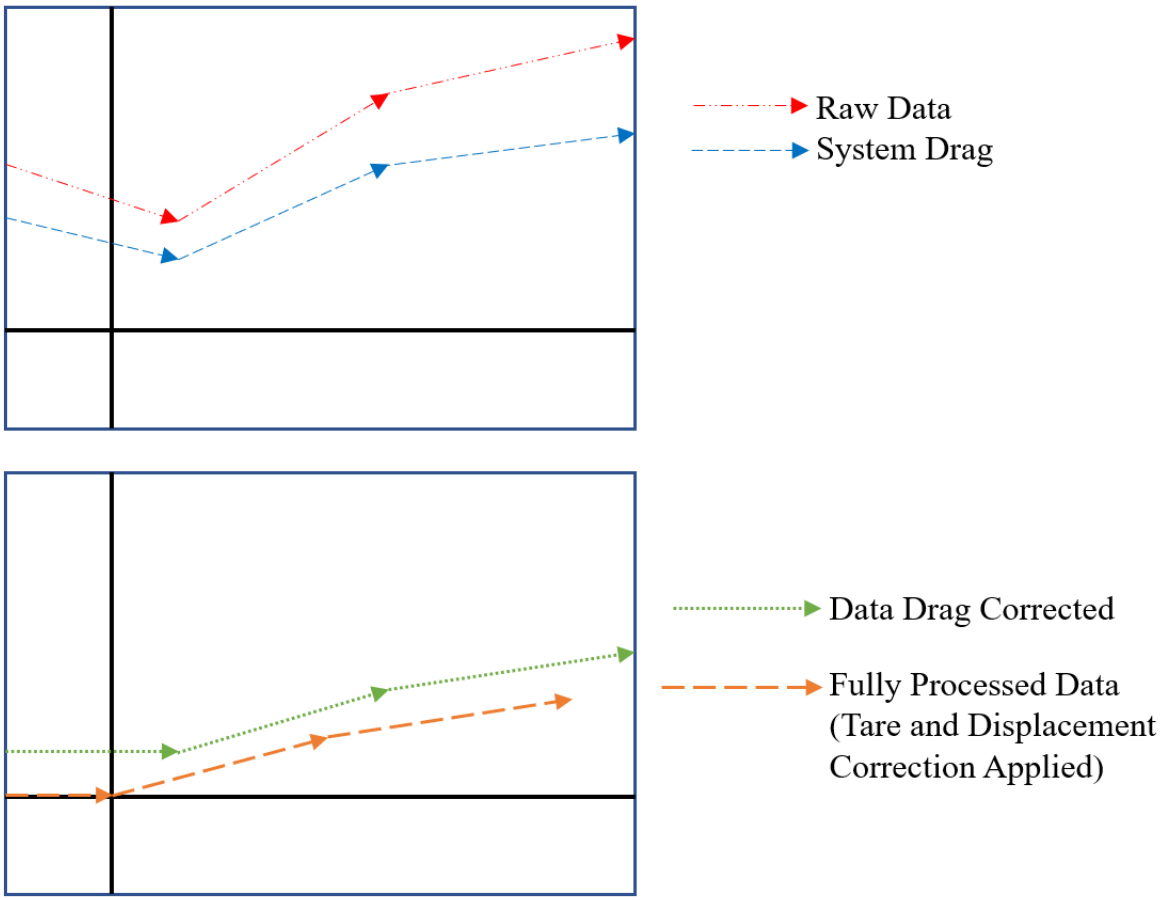

Figure 4.2 Visual representation of data processing.

Curve (1) represents the raw data. Curve (2) shows the data collected with no specimen, representing only the inherent drag in the system. Curve (3) shows the raw data with the drag removed via superposition. Curve (4) shows the final zeroed data after taring and setting the point of contact to the origin.

After switching from intentation testing to the rotary assembly new data were collected, the initial test runs were cloesly evaluated to help ensure the test apparatus was working as intended. The gathered rotary data were highly effected by a small misalignment of the rotary head which resulted in oscillatory increasing data. This was smoothed with the matlab rlowess function, which is a robust linear fit method, using a 20 point span.

Chapter 5: Results

5.1 Indentation

The main body of work focused on indentation testing and data collection methods. The only directly comparible work was that of Trepp (1958). An overlay of this study's data on top of Trepp's work is provided in Figure 5.1. To provide hardness data points for comparison, an indentation depth of 3 mm was selected. This depth was chosen based on the appearance of load drops in the data and the diameter of the probes. Data were pulled from each force vs displacement curve at that depth from initial indentation. Data points from each run were included for the sake of completeness.

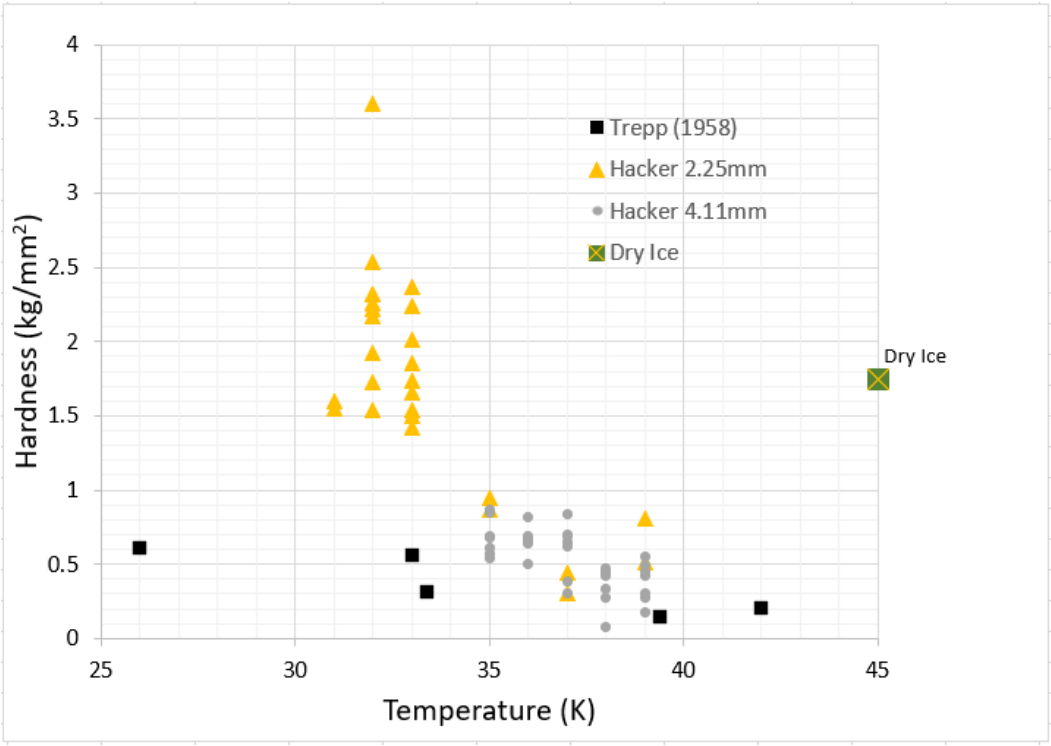

Figure 5.1. Hacker vs. Trepp data plot, multiple indenter diameters (mm) shown.

Averages from each temperature run are shown with deliniation between the sweep run (indents at different temperatures from a single sample), and full runs at a given temperature (see Figure 5.2). All data were initially drag corrected. For visual clarity of the data only every 15th point is displayed. All plots use the same X and Y axis limits with included legends to provide information relivent to each plot. Indentor diameter is included in the legend for every run, optional information includes rotary position, listed as "P#", temperature, and notation for sweep or constant temperature across runs.

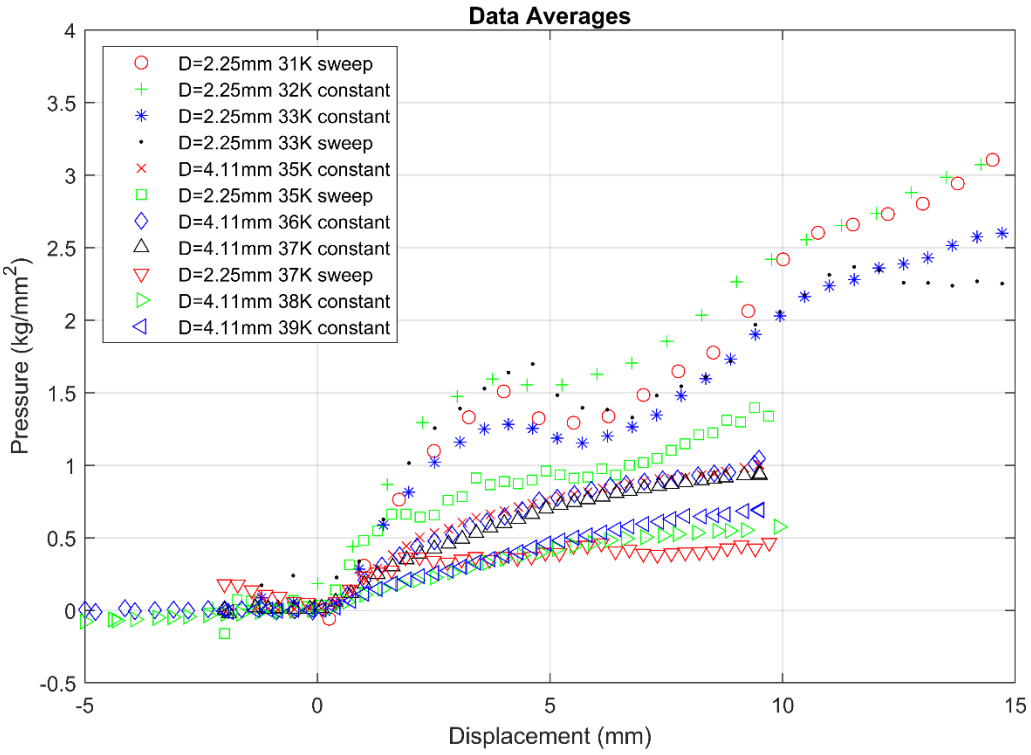

Figure 5.2. Data Averages.

To provide an additional comparison plot, representative runs from 31 K to 39 K were overlaid to provide visual comparison (see Figure 5.3). The side by side comparison highlights the behavior difference between the lower and upper range of the tested temperatures. Below 35 K a rise in preasure, break, then continuing to rise in pressure contrasts the smooth increase at and above 35 K.

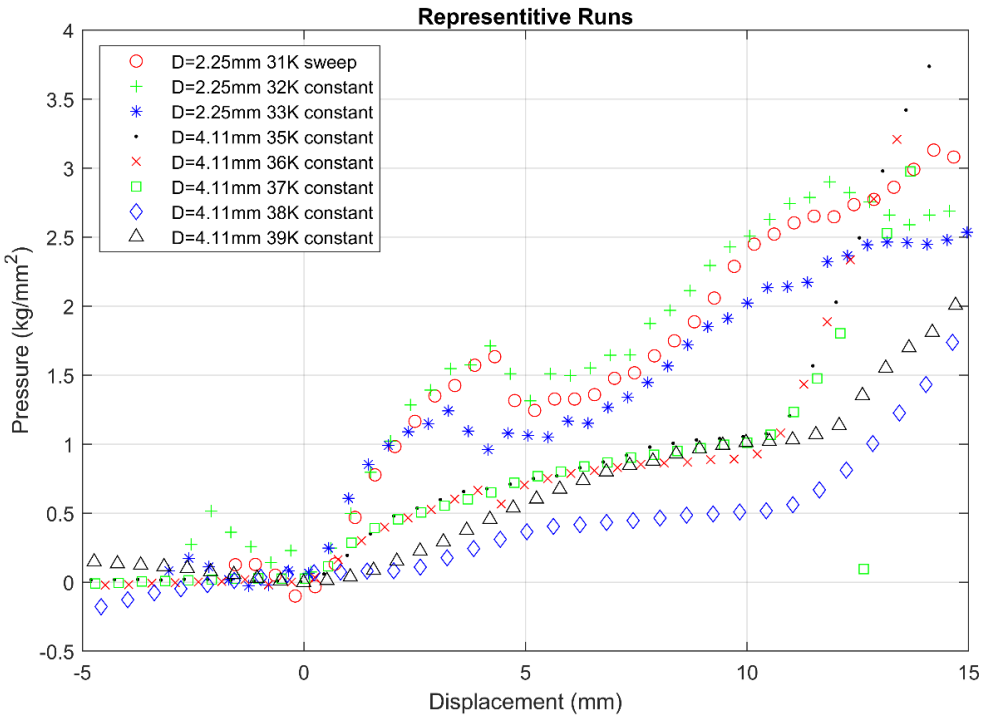

Figure 5.3. Representative runs from 31 K to 39 K.

Plots are listed in order of increasing temperature starting at 31 K and proceeding through 39 K. Plots are broken into two sections, those below 35 K, and above, with generalized behavior explanations before each grouping.

Figures 5.4 through 5.6 all use a 2.25 mm indenter, and show a distinct rise, fall, then rise again behavior. The first two Figures have temperature indications, with Figure 5.4 temperature was recorded immediately after the run. In Figure 5.5 temperature was recorded immediately before and after the runs, with the correspondingly listed with the first and last run.

The data at 33 K (Figure 5.6) overlays data taken at two different points in time using the same diameter indenter. As previously indicated the runs notated as sweep were data at multiple temperatures taken from a single sample after stabilizing at each temperature. The rotational positions are the same as both sets of data were taken using the same 2.25 mm indenter.

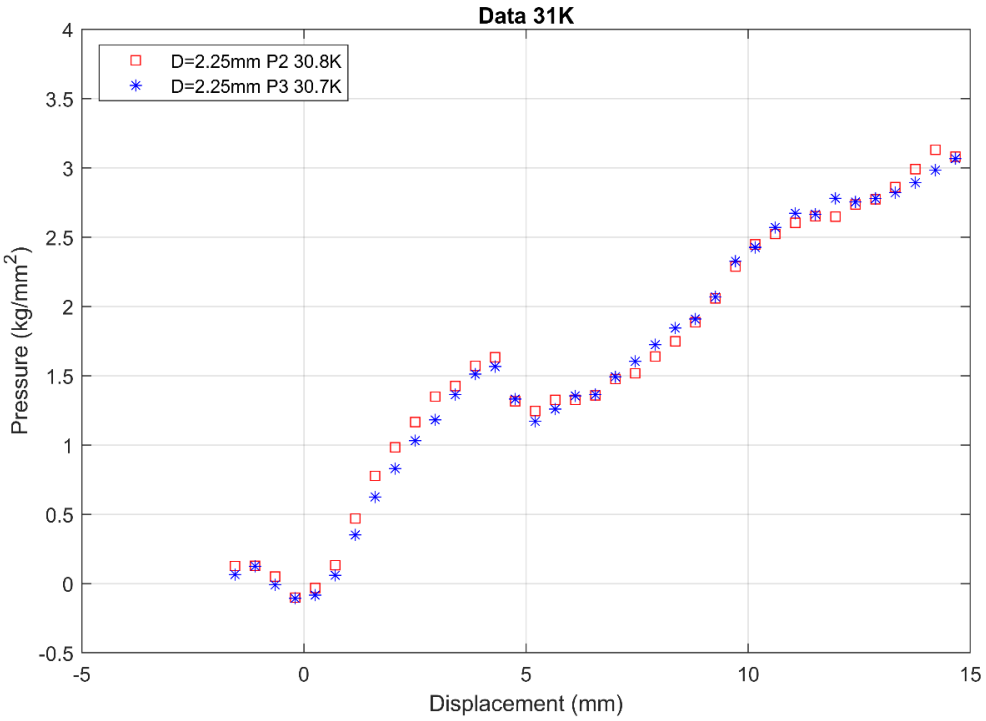

Figure 5.4 Indenter data at 31 K at positions 2 and 3.

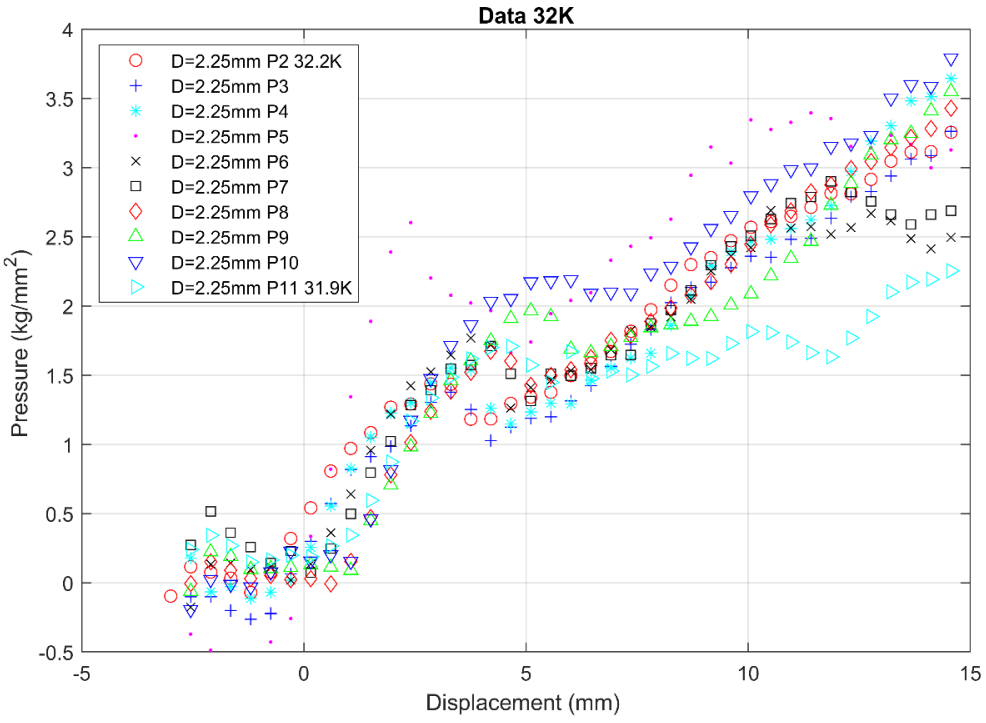

Figure 5.5 Indenter data at 32 K.

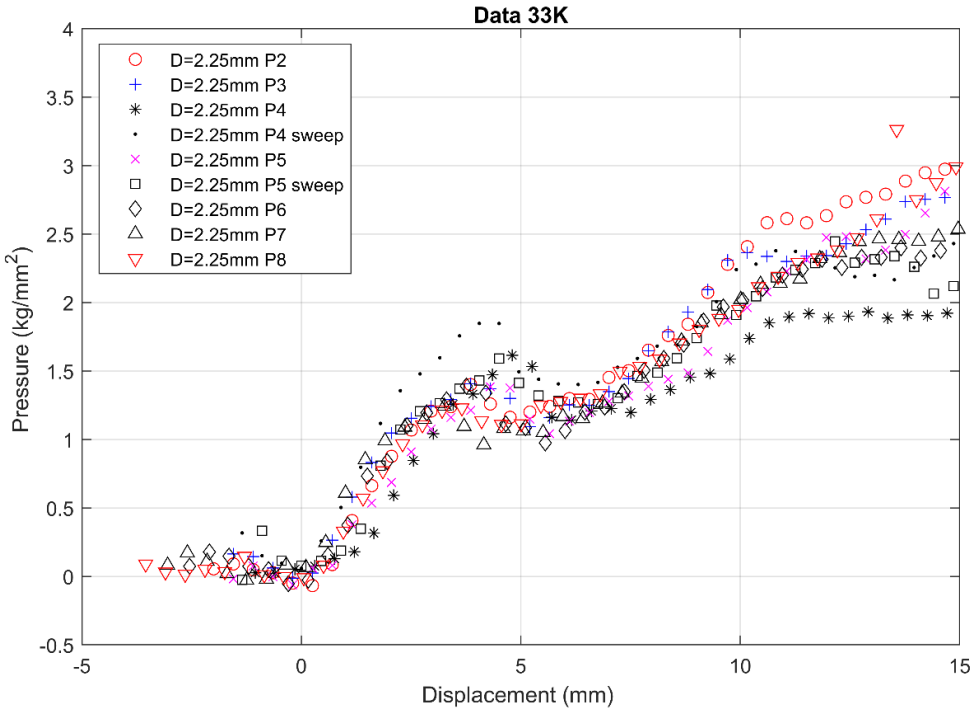

Figure 5.6 Indenter data at 33 K.

Figures 5.7 through 5.11 are below, they represent data from 35 K though 39 K. The plots demonstrate a visibly smoother profile across the indent range as compared to the previous Figures. This range primarily used the larger 4.11 mm diameter indenter though some data was taken with the smaller 2.25 mm indenter and can be used for comparison. The rotary positions are not directly comparable between the two sizes as the 4.11mm indenter used eight evenly spaced rotary positions as opposed to the eleven positions for the 2.25mm indenter.

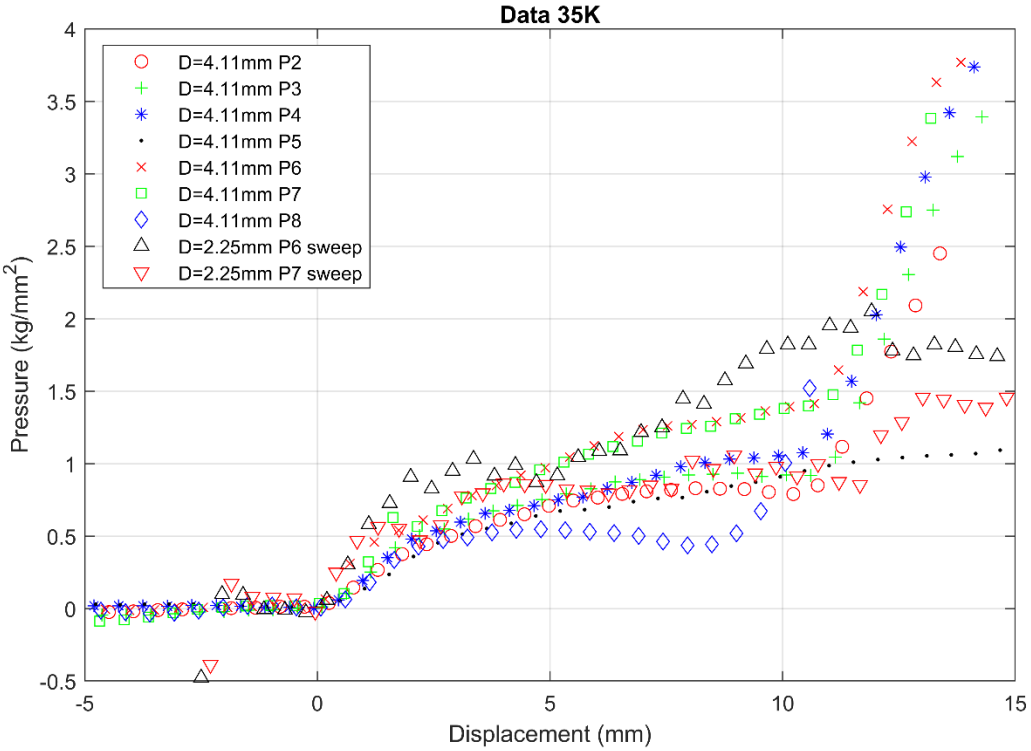

Figure 5.7 Indenter data at 35 K.

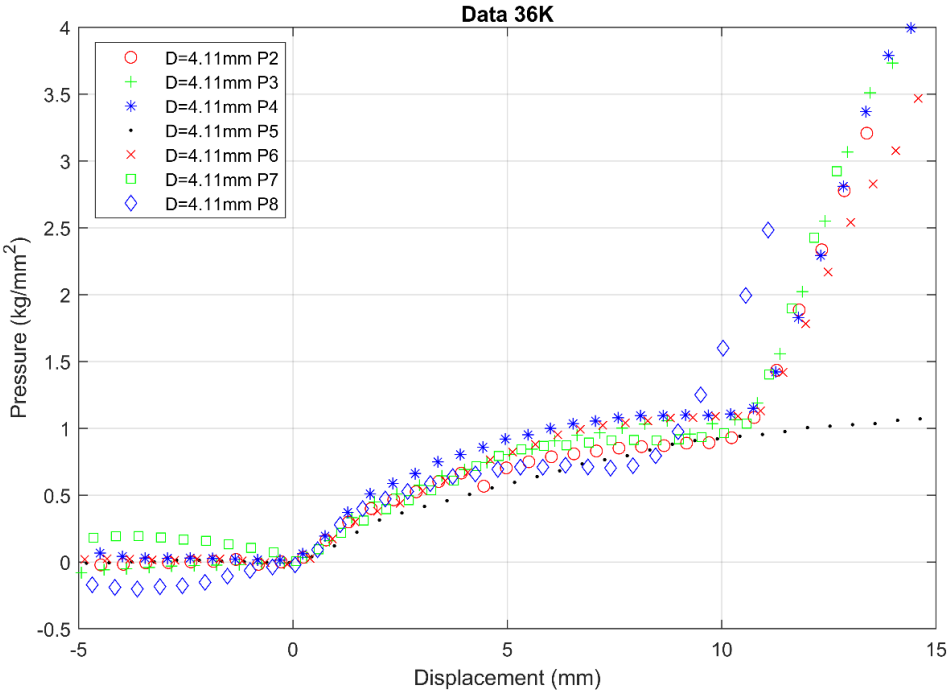

Figure 5.8 Indenter data at 36 K.

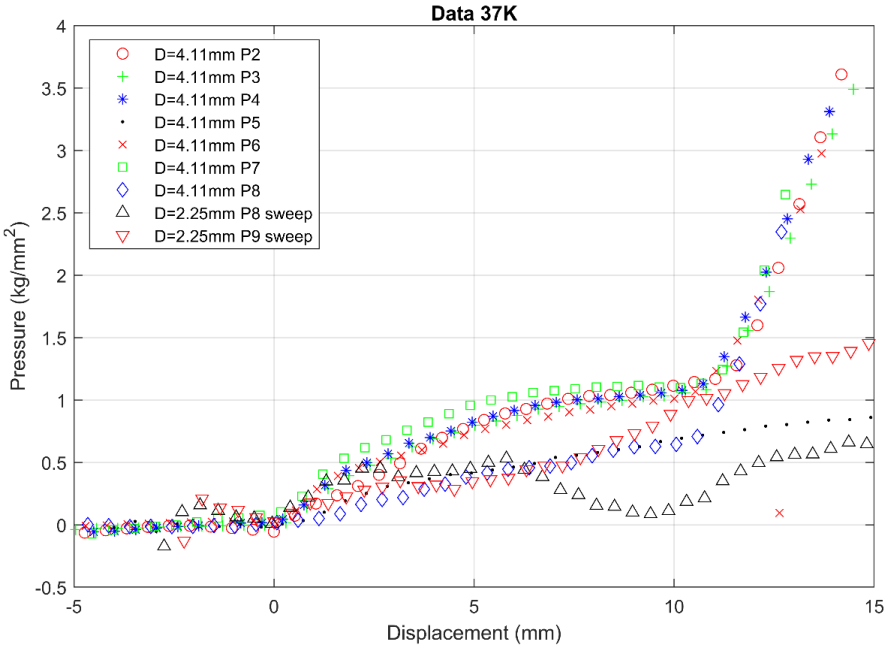

Figure 5.9 Indenter data at 37 K, note two indenter sizes used.

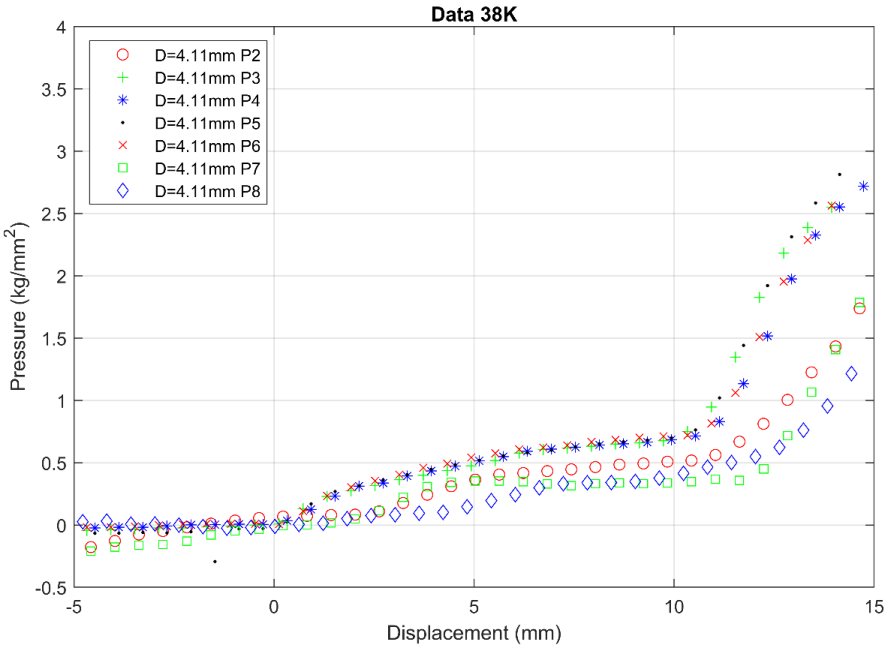

Figure 5.10 Indenter data at 38 K.

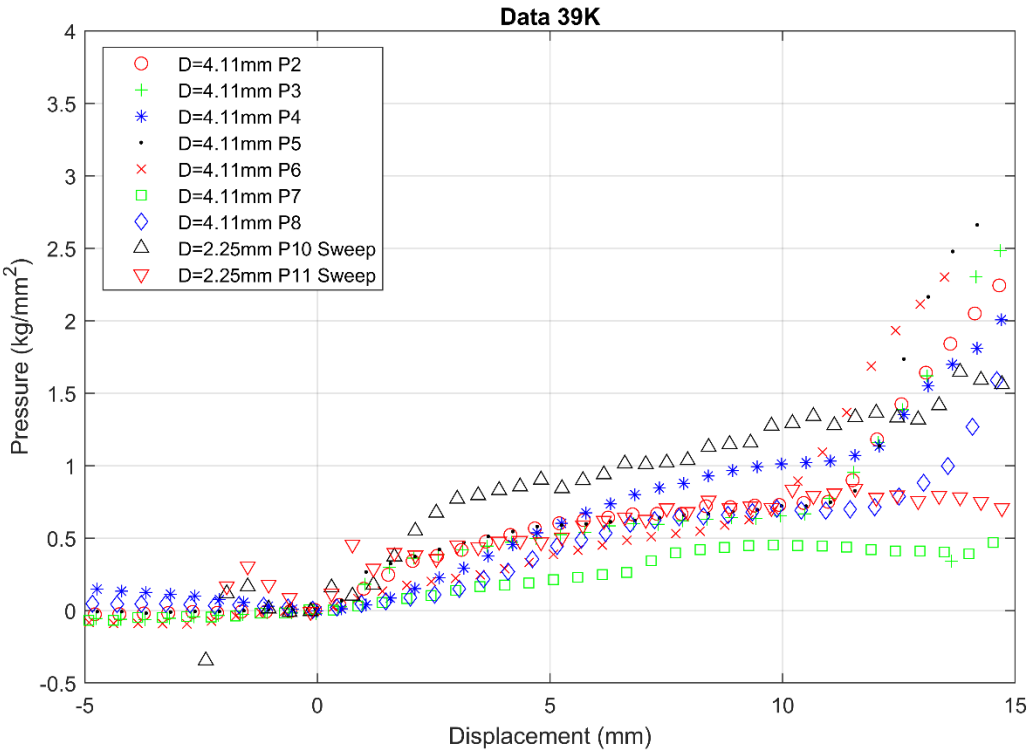

Figure 5.11 Indenter data at 39 K.

To provide reference Figure 5.12 is included to show a full indent cycle. This plot contains no drag correction, force taring, or zero offset adjustment. This is included to show the raw data with the process of the indent following a clockwise motion. The run starts at 22 mm and has a positive pressure reading while the indenter is moving down to a max depth of 52 mm. After reaching 52mm the indenter changes direction to return to the starting displacement, at which point the pressure reading becomes negative.

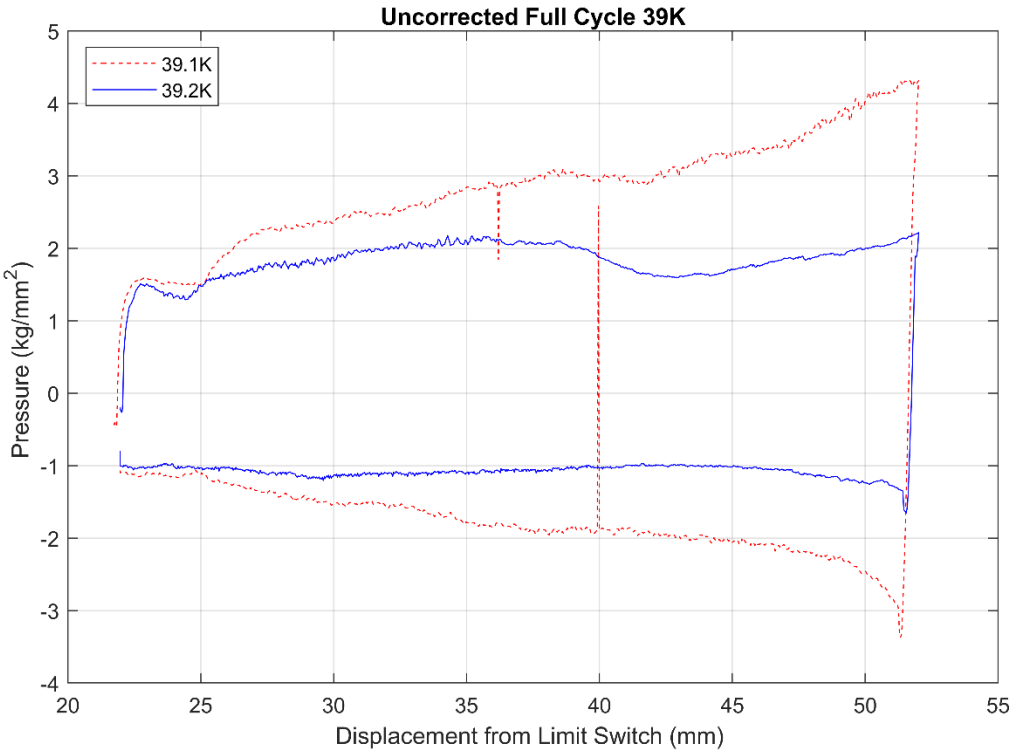

Figure 5.12 Uncorrected full cycle runs at 39 K.

5.2 Rotary

Mechanical rotary runs were completed at 32 K and 33 K. The plot shows both pressure on the tooth face and vertical force (normal to the ice surface) plotted against displacement (see Figure 5.12).

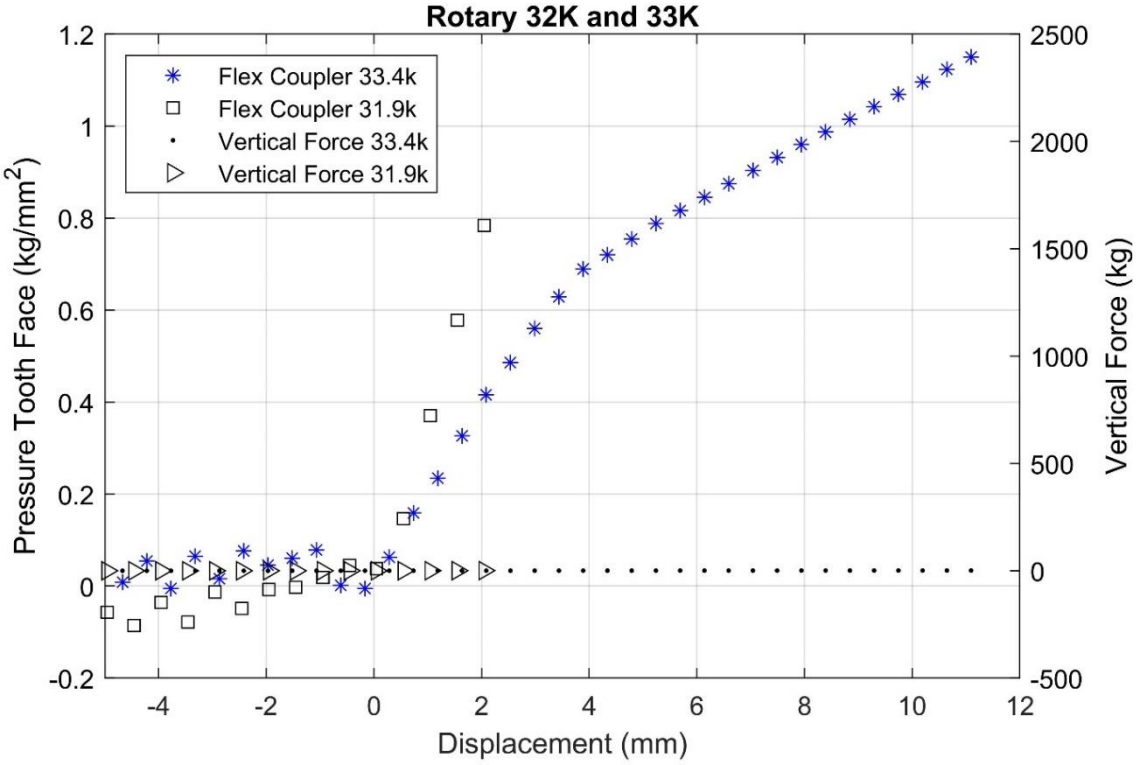

Figure 5.13 Rotary data.

Chapter 6: Discussion

Before plotting the pressure vs. displacement curves it was expected, given the flat punch indentors used, that after the point of impact force would rise, taper off, and enter steady state. In typical solids at room temperature, a sample's hardness is defined as the steady state value. Plotting the pressure vs. displacement from data initially collected did not match the expected results. Instead, two temperature dependent behaviors were observed. In samples at or below 35 K, after indenter impact with the sample, a sharp rise in pressure would occur followed by a slight dropoff, then continual rise through the length of indentation. In samples above 35 K, there was no dropoff and instead a more gradual rise in pressure was observed. Interestingly, the behavior split corresponds with the alpha to beta phase transition temperature of 35.6 K [22]. With the alpha phase samples, at 35 K and below, it is believed that a brittle failure mode explains the behavior; however, this is not fully verifiable without further testing as no direct observation took place. The plots at 35 K didn't show the presumed brittle fracture event with the same severity as the 31 to 34 K plots. Solid hydrogen cryocrystals have shown phase change driven by mechanical deformation [23]. The same phenomenon may be occuring in the SN_2, such that under 35.6 K with deformation nitrogen may change from its alpha to beta phase, which may explain the behavior shown in the 35 K plot. There is also a large disparity in hardness across the temperature range, with hardness increasing by a factor at least four over the full range. Tempeature dependence appears both above and belowthe transition temperature with possibly a large step at the phase point. The existence of both brittle and compressible behaviors complicate the Triton Hopper project from both design and mission planning prespectives. Mechaninisms for gathering SN_2 along with ground contact pads for supporting the craft will need to consider both behaviors along with the considerable change in hardness across the temperature range.

Because the indentation pressure did not reach a steady state, a depth needed to be assumed to pull hardness values. Visual analysis of plots at and below 35 K showed the presumed brittle failure to occure at a depth of 3 mm, which was selected as the depth to represent hardness. Data from depths greater than 3 mm had the potential to be from a cracked specimen and thus would not be a consistent representation of the material. The selected depth is especially useful for comparisons across the temperature range.

With depth selected, the captured hardness values could be compared to Trepp's [2] work. At the chosen depth of 3 mm hardness values were significantly harder than Trepp's work, with the disparity increasing at lower temperature. There are several hypotheses that may partially or completely

explain the differences. The first is heat transfer related; Trepp used a conical stainless steel indentor, and while the work was excellent, the indenter may not have been adequately precooled, thus heating the sample slightly during indentation. This would skew the SN_2 data as hardness is shown to be highly temperature dependent. The second hypothesis is a function of the sample creation method. Trepp's SN_2 sample was formed via evaporitive cooling from liquid nitrogen. This method is likely to have left small voids in solid sample, thus forming an SN_2 foam. Comparatively this study's cryocooler formed sample should be completely solid because the heat was directly and slowly removed with no material loss. The cryocooler-created sample should not contain any voids and few if any cracks given the slow cooling rate, though such has not been confirmed. The lack of voids would likely increase the hardness, and the density between the two samples would not be the same. The third hypothesis is that the results simply may not be directly comparible because of the differing indentor geometries. Conical indentation inherently imposes a cutting action on the material, whereas, the flat punch geometry does not. Thus, conical indentation and punch indentation represent slightly different deformation mechanisms which are not well understood for cryogenic solids. Further research into each of these theories should take place but are beyond the scope of this work.

Early in testing data procesing were started, visual inspection of plots showed that the displacement at which the indenter impacted the sample didn't always match the expected displacemnt value. This may be a result of hot filling the smaller mearured cylinder, e.g. the small cylinder was filled then immediately emptied without allowing time for the N_2 temperature to equlibriate. Slight deviations in sample height should not have any effect on results as interaction effects between the SN_2 indenter and sample cup are not anticipated with the seperation between indenter and sample cup.

The rotary work showed viability of mechanical gathering methods. If the Triton Hopper project, or other similar project, require the mechanical gathering of cryocrystals it is highly recommended that this work be refined and continued.

In looking at ways the data could be wrong there are the potential errors of inadequate calibration and friction between the sample and indenter due to the parallel sides of the flat punch geometry. Using springs as discussed in section 3.4 provided adequate calibration to show that both the mechanism and data processing routine matched expected values. Regarding potential friction it would be expected that this would be equal during indentation and retraction. Figure 5.12 shows a complete indentation cycle, it shows a slight additional drop in measured force after the change in direction, then consistent behavior during retraction. If friction between the indenter and sample was

significant, a large change in readings would occur when the indenter was no longer in contact with the SN_2 sample, this was however not the case. Without notable change any effect on the data due to friction should be negligible.

After completion of this project and learning more about cryogenics in general there are a handful of suggestions for future iterations of this and/or similar type projects. The first is regarding the dynamic sealing of the system. While the double O-ring provided a good seal, the non-linear drag and hysteresis at direction change were detrimental. Obtaining a higher tolerance level on the sealing block and a substantially finer polish on the rod would help substantially. Similar setups exist in nanoindentation machines, so the seal design type is a known good. Some of the drag experienced may have been due to the high viscosity of the Dow Corning high-vacuum grease. Specifically, when the shaft was raised some of the grease may have gone under its minimum temperature rating of -40°C which may have played a role in the high drag loads as the temperature dependency is not known. Changing the design to incorporate vacuum baffles may be a preferred option It was discovered late in the project that vacuum baffles exist in diametral sizing and sufficient range of motion to allow for indentation. Using baffles should provide more consistent force readings with a finer accuracy potential. Ideally force unloading curves could be taken, allowing for modulus of elasticity to be calculated.

While the rotary mechanism worked to give readings, the nature of the device required it to be perfectly lined up without flex on the part of the shaft, which was challenging to achieve. The dynamometer test numbers should thus only be taken as a rough guide. While the dynamometer concept developed was proven, the implementation needs refinement and further testing to validate.

To improve the passthrough for rotational motion, two idea paths are presented as follows. The first is to continue with the dual O-rings, keeping them located at or near room temperature and mounted in such a way that they are used solely for rotational motion. The second, and preferred option, is to use ferrofluidic rotating seals. While substantially more expensive, ferrofluidic seals are the preferred method for any setup that required continual rotational motion. Either the O-ring or ferrofluidic seal-based option should still use a baffle system for allowing vertical motion. These changes would work well for both dynamometer and indentation work.

Chapter 7: Conclusion

This project represents some of the only indentation work with cryocrystals. Flat punch indentation techniques were shown to work with solidified nitrogen. The data collected indicate that SN_2 is harder than historic testing and that a simple hardness value is not sufficient to describe the material at a given temperature. The response to indentation is also highly temperature dependent with clearly identifiable behavior differentiation between the alpha and beta phases. Rotary testing demonstrated that mechanical gathering should be achievable given the correct design parameters. This work also shows the need for further and expanded testing of cryocrystals. This need will only expand as Triton Hopper, for which this project was completed, and other projects continue to explore the outer reaches of our solar system.

References

[1] D. Sagmiller and J. Hartwig, “Survey of Cryogenic Nitrogen Thermo-Mechanical Property Data Relevant to Outer Solar System Bodies,” *Earth Space Sci.*, Jul. 2020, doi: 10.1029/2019EA000640.

[2] C. Trepp, “Die Härte von N-2, O-2, Ar und von N-2-O-2-Gemischen,” ETH Zurich, 1958. doi: 10.3929/ETHZ-A-000097525.

[3] A. V. Leonteva, Yu. S. Stroilov, and I. N. Krupskii, “Fiz. Kondens. Sostoyan,” *Nat Acad Sci*, vol. XVI, 1971.

[4] Y. Yamashita, M. Kato, and M. Arakawa, “Experimental study on the rheological properties of polycrystalline solid nitrogen and methane: Implications for tectonic processes on Triton,” *Icarus*, vol. 207, no. 2, pp. 972–977, Jun. 2010, doi: 10.1016/j.icarus.2009.11.032.

[5] D. Williams, “Ranger to the Moon (1961 - 1965).” https://nssdc.gsfc.nasa.gov/planetary/lunar/ranger.html (accessed Jul. 26, 2021).

[6] D. Williams, “Surveyor to the Moon (1966 - 1968).” https://nssdc.gsfc.nasa.gov/planetary/lunar/surveyor.html (accessed Jul. 26, 2021).

[7] D. P. Cruikshank, R. Hamilton Brown, and R. N. Clark, “Nitrogen on Triton,” *Icarus*, vol. 58, no. 2, pp. 293–305, May 1984, doi: 10.1016/0019-1035(84)90046-0.

[8] A. L. Broadfoot *et al.*, “Ultraviolet spectrometer observations of Neptune and Triton,” *Science*, vol. 246, pp. 1459–1466, Dec. 1989, doi: 10.1126/science.246.4936.1459.

[9] B. Conrath *et al.*, “Infrared observations of the neptunian system,” *Science*, vol. 246, no. 4936, pp. 1454–1459, Dec. 1989, doi: 10.1126/science.246.4936.1454.

[10] E. Quirico *et al.*, “Composition, Physical State, and Distribution of Ices at the Surface of Triton,” *Icarus*, vol. 139, no. 2, pp. 159–178, Jun. 1999, doi: 10.1006/icar.1999.6111.

[11] L. A. Soderblom *et al.*, “Triton’s Geyser-Like Plumes: Discovery and Basic Characterization,” *Science*, vol. 250, no. 4979, pp. 410–415, Oct. 1990, doi: 10.1126/science.250.4979.410.

[12] P. C. Thomas, “The Shape of Triton from Limb Profiles,” *Icarus*, vol. 148, no. 2, pp. 587–588, Dec. 2000, doi: 10.1006/icar.2000.6511.

[13] S. Oleson and G. Landis, “Triton Hopper: Exploring Neptune’s Captured Kuiper Belt Object,” Glenn Research Center, Cleveland, Ohio, TM, 2018. [Online]. Available: https://strives-uploads-prod.s3.us-gov-west-1.amazonaws.com/20180001294/20180001294.pdf?AWSAccessKeyId=AKIASEVSKC45ZTTM42XZ&Expires=1598573044&Signature=SSC95yE3T3LLHVjE%2BhSnMTrXT0c%3D

[14] “Pluto,” *NASA Solar System Exploration*. https://solarsystem.nasa.gov/planets/dwarf-planets/pluto/overview (accessed Sep. 04, 2021).

[15] “In Depth | Neptune,” *NASA Solar System Exploration*. https://solarsystem.nasa.gov/planets/neptune/in-depth (accessed Sep. 04, 2021).

[16] R. Radebaugh, “Cryogenics,” *The MacMillan Encyclopedia Of Chemistry*. 2002. [Online]. Available: https://trc.nist.gov/cryogenics/aboutCryogenicsII.pdf

[17] “Multi layer Insulation & Multilayer Film Materials | Dunmore,” *Dunmore*. https://www.dunmore.com/products/multi-layer-films.html (accessed Aug. 27, 2020).

[18] S. Kalpakjian and S. R. Schmid, *Manufacturing Processes for engineering materials*, 6th ed. Pearson, 2018.

[19] A. C. Fischer-Cripps, *Nanoindentation*, Third. Springer, 2011.

[20] I. A. Richardson, “Characterizing Dissolved Gasses in Cryogenic Liquid fuels,” disseratation, Washington State University, 2017.

[21] P. Hannifin, *Parker O-ring Handbook*. Parker Hannifin Corporation O-ring Division, 2007. [Online]. Available: https://www.parker.com/literature/Parker_O-Ring_Handbook.pdf

[22] V. G. Manzheliĭ and Y. A. Freiman, *Physics of cryocrystals*. Woodbury, NY: American Institute of Physics, 1997.

[23] J. Leachman, J. Pfotenhauer, and G. Nellis, “Dynamic shear stress and heat transfer of solid hydrogen, deuterium, and neon,” *J. Appl. Phys.*, vol. 111, no. 8, p. 083513, Apr. 2012, doi: 10.1063/1.3703566.

Appendix A - Equipment List

Lakeshore Cryotronics 336 Temperature Controller

Mark 10 ES-20 Load Frame (modified)

Custom Indenter

Custom Rotary Apparatus

Leybold DB8 rotary vain vacuum pump

Agilent Tv 81m turbomolecular pump

WSU HYPER Lab Custom Cryostat

CRYOMECH PT405 cryocooler with water cooled CPA 2850 compressor

Cryogenic Control Systems S950-BB RTD (Located on Bus Bar)

Lakeshore Cryotronics PT-100 RTD (Located on Indenter)

CALT DYLE-103 30KG Load cell

HX711 Load Cell Amplifiers

Arduino Mini

TMC5160 SilentStepStick

NEMA 23 Stepper Motor

Custom Electronics Breakout Board

Appendix B - Additional Dry Ice Data and Spring Validation Plots

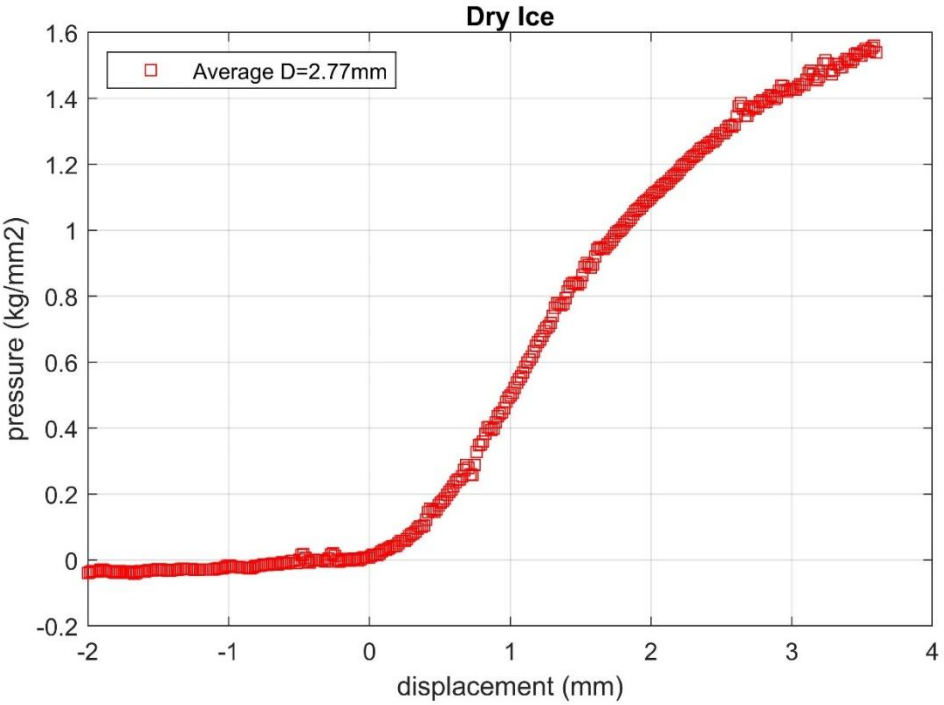

Figure B.1. Combined Average of all Dry Ice Runs.

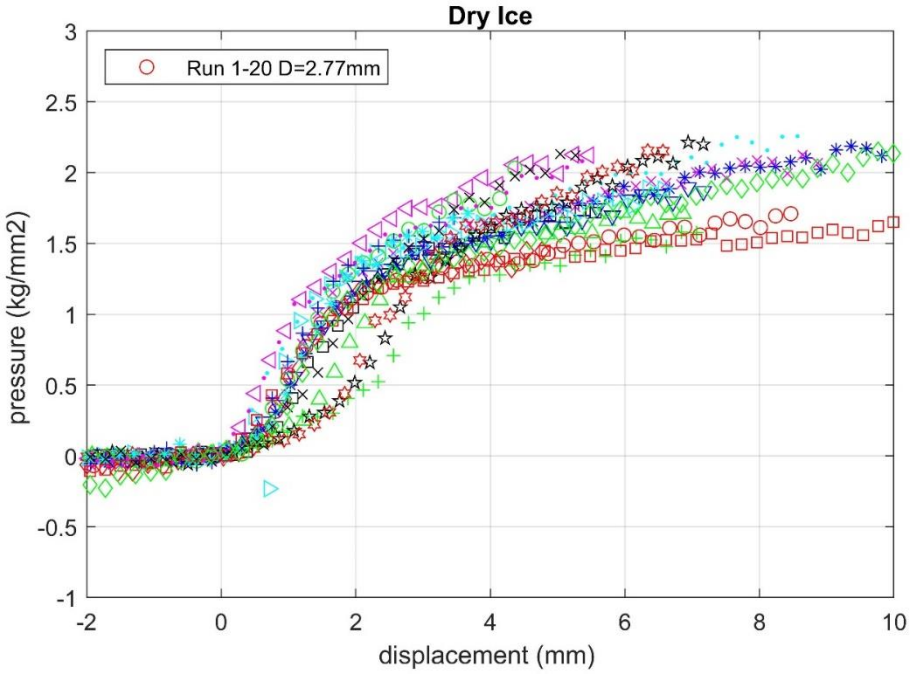

Figure B.2. All Dry Ice Runs.

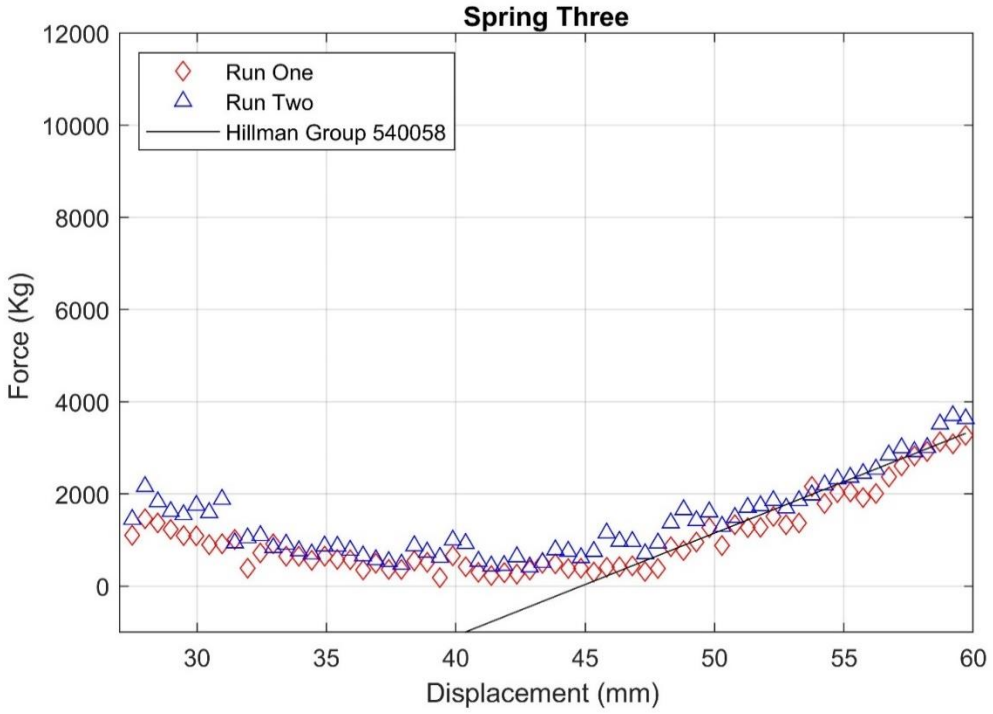

Figure B.3. Spring Three, Hillman 540058 for Verification.

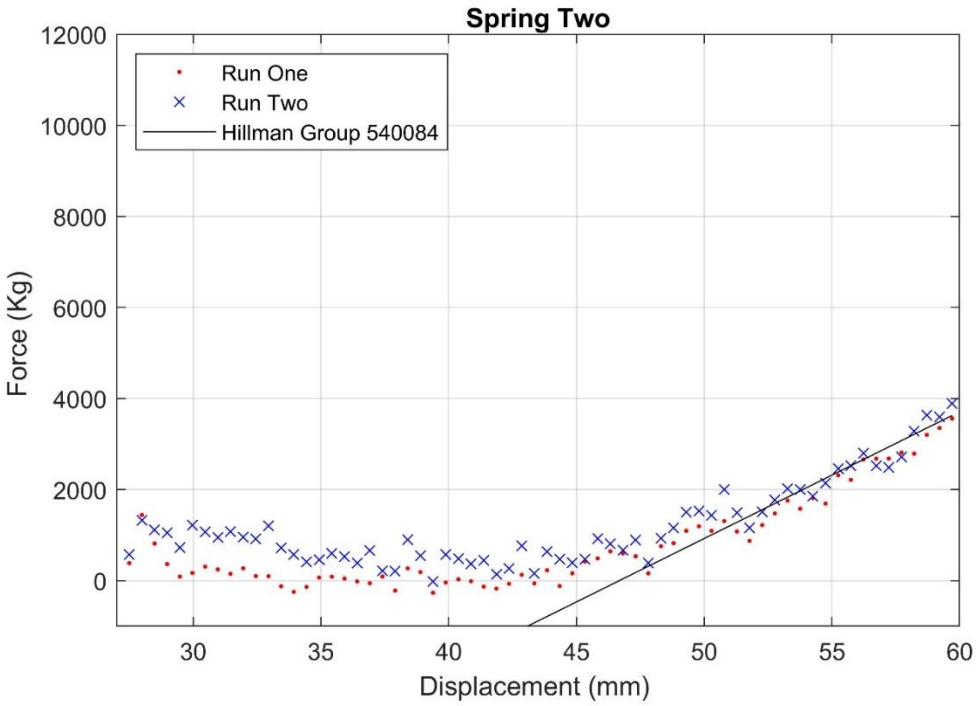

Figure B.4. Spring Two, Hillman 540084 for Verification.

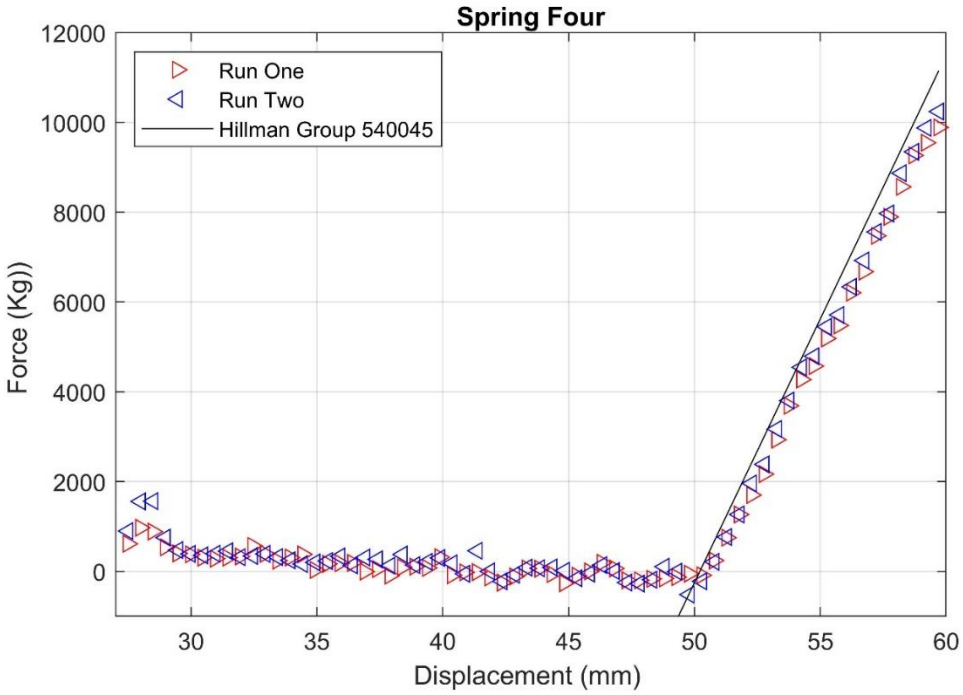

Figure B.5. Spring Four, Hillman 540045 for Verification.

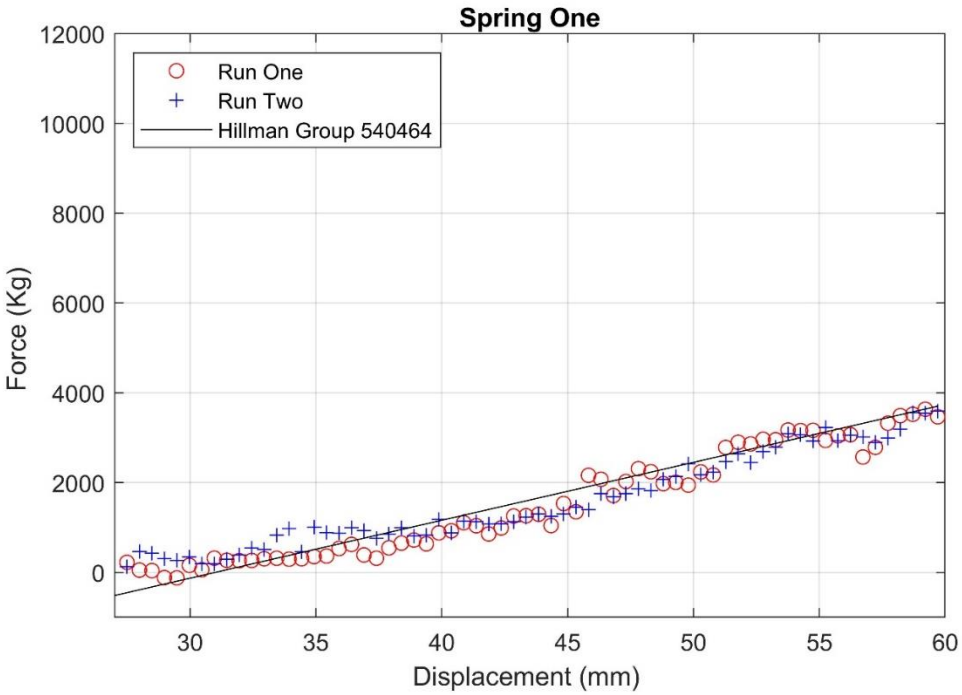

Figure B.6. Spring One, Hillman 540464 for Verification.

Appendix C - MATLAB Processing Example Code

The following code was written for use with the large 4.11mm indenter at 39 K. Other processing code is of the same structure with changes to select the correct txt files and label plots correctly.

```
%Masters data work
%Zachary Hacker
%1/06/2020
%large indenter runs
%for 39k december 19th gathered data



clc
close all
clear all



n=15;
x=(linspace(15,50,1000))';

%%%%%%%%%%%%%%%%%%%%%%%%%%%%%%%%%%%%%%%%%%%%%%%%%
%%%%%%%%%%%%%%%%%
%2.25mm dia indenter
%force from indentor
%
str1=fopen('39kp10.txt');
cell1=textscan(str1,'%{HH:mm:ss.SSS}D ->%f,%f');%,'Delimiter','->');
fclose(str1);
force1=cell2mat(cell1(2));
disp1=cell2mat(cell1(3));
i2=find(disp1>22 &disp1<23);
j2=find(disp1>=52);
```

```
forceten=interpft(force1(i2(1):j2(1)),1000)*(0.001*4/(pi*2.25^2));


str1=fopen('39kp11.txt');
cell=textscan(str1,'%{HH:mm:ss.SSS}D ->%f,%f');%,'Delimiter','->');
fclose(str1);
force2=cell2mat(cell(2));
disp2=cell2mat(cell(3));
i2=find(disp2>22 &disp2<23);
j2=find(disp2>=52);
forceeleven=interpft(force2(i2(1):j2(1)),1000)*(0.001*4/(pi*2.25^2));

%drag force


%p10 run 1
%
str1=fopen('zeroP10R1.txt');
cell=textscan(str1,'%{HH:mm:ss.SSS}D ->%f,%f');%,'Delimiter','->');
fclose(str1);
force2=cell2mat(cell(2));
disp3=cell2mat(cell(3));
i2=find(disp3>22 &disp3<23);
j2=find(disp3>=52);
z1=interpft(force2(i2(1):j2(1)),1000)*(0.001*4/(pi*2.25^2));


%p10 run 2
%
str1=fopen('zeroP10R2.txt');
cell=textscan(str1,'%{HH:mm:ss.SSS}D ->%f,%f');%,'Delimiter','->');
fclose(str1);
force2=cell2mat(cell(2));
```

```
disp4=cell2mat(cell(3));
i2=find(disp4>22 &disp4<23);
j2=find(disp4>=52);
z2=interpft(force2(i2(1):j2(1)),1000)*(0.001*4/(pi*2.25^2));


p2=(z1+z2)/2;


f10cr=forceten-p2;


%p11 run 1
%
str1=fopen('zeroP11R1.txt');
cell=textscan(str1,'%{HH:mm:ss.SSS}D ->%f,%f');%,'Delimiter','->');
fclose(str1);
force2=cell2mat(cell(2));
disp5=cell2mat(cell(3));
i2=find(disp5>22 &disp5<23);
j2=find(disp5>=52);
z3=interpft(force2(i2(1):j2(1)),1000)*(0.001*4/(pi*2.25^2));


%p11 run 2
%
str1=fopen('zeroP11R2.txt');
cell=textscan(str1,'%{HH:mm:ss.SSS}D ->%f,%f');%,'Delimiter','->');
fclose(str1);
force2=cell2mat(cell(2));
disp6=cell2mat(cell(3));
i2=find(disp6>22 &disp6<23);
j2=find(disp6>=52);
```

```
z4=interpft(force2(i2(1):j2(1)),1000)*(0.001*4/(pi*2.25^2));

p3=(z3+z4)/2;

f11cr=forceeleven-p3;



%%%%%%%%%%%%%%%%%%%%%%%%%%%%%%%%%%%%%%%%%%%%%%%%%%%%%%%%%%%%%%%%%%%%%%%%%%%%%%%%%%%%%%%%%%%%%%%%%%%%
%4.11mm dia indenter

str1=fopen('39kbigr2.txt');
cell1=textscan(str1,'%{HH:mm:ss.SSS}D ->%f,%f,%f');%,'Delimiter','->');
fclose(str1);
force=cell2mat(cell1(2));
displacementTwo=cell2mat(cell1(3));
i2=find(displacementTwo>15 &displacementTwo<16);
j2=find(displacementTwo>=50);
forcePTwo=-interpft(force(i2(1):j2(1)),1000)*(0.001*4/(pi*4.11^2));

str1=fopen('39kbigr3.txt');
cell1=textscan(str1,'%{HH:mm:ss.SSS}D ->%f,%f,%f');%,'Delimiter','->');
fclose(str1);
force=cell2mat(cell1(2));
displacementThree=cell2mat(cell1(3));
i3=find(displacementThree>15 &displacementThree<16);
j3=find(displacementThree>=50);
forcePThree=-interpft(force(i3(1):j3(1)),1000)*(0.001*4/(pi*4.11^2));

str1=fopen('39kbigr4.txt');
cell1=textscan(str1,'%{HH:mm:ss.SSS}D ->%f,%f,%f');%,'Delimiter','->');
fclose(str1);
force=cell2mat(cell1(2));
```

```
displacementFour=cell2mat(cell1(3));
i4=find(displacementFour>15 &displacementFour<16);
j4=find(displacementFour>=50);
forcePFour=-interpft(force(i4(1):j4(1)),1000)*(0.001*4/(pi*4.11^2));

str1=fopen('39kbigr5.txt');
cell1=textscan(str1,'%{HH:mm:ss.SSS}D ->%f,%f,%f');%,'Delimiter','->');
fclose(str1);
force=cell2mat(cell1(2));
displacementFive=cell2mat(cell1(3));
i5=find(displacementTwo>15 &displacementTwo<16);
j5=find(displacementFive>=50);
forcePFive=-interpft(force(i5(1):j5(1)),1000)*(0.001*4/(pi*4.11^2));

str1=fopen('39kbigr6.txt');
cell1=textscan(str1,'%{HH:mm:ss.SSS}D ->%f,%f,%f');%,'Delimiter','->');
fclose(str1);
force=cell2mat(cell1(2));
displacementSix=cell2mat(cell1(3));
i6=find(displacementSix>15 & displacementSix<16);
j6=find(displacementSix>=50);
forcePSix=-interpft(force(i6(1):j6(1)),1000)*(0.001*4/(pi*4.11^2));

str1=fopen('39kbigr7.txt');
cell1=textscan(str1,'%{HH:mm:ss.SSS}D ->%f,%f,%f');%,'Delimiter','->');
fclose(str1);
force=cell2mat(cell1(2));
displacementSeven=cell2mat(cell1(3));
i7=find(displacementSeven>15 &displacementSeven<16);
j7=find(displacementSeven>=50);
forcePSeven=-interpft(force(i7(1):j7(1)),1000)*(0.001*4/(pi*4.11^2));

str1=fopen('39kbigr8.txt');
```

```
cell1=textscan(str1,'%{HH:mm:ss.SSS}D ->%f,%f,%f');%,'Delimiter','->');
fclose(str1);
force=cell2mat(cell1(2));
displacementEight=cell2mat(cell1(3));
i8=find(displacementEight>15 &displacementEight<16);
j8=find(displacementEight>=50);
forcePEight=-interpft(force(i8(1):j8(1)),1000)*(0.001*4/(pi*4.11^2));


%%%%%%%%%%%%%%%%%%%%%%%%%%%%%%%%%%%%%%%%%%%%%%%%%%%%%
%%%%%%%%%%%%%%%%%%%

%force taring
forcePTwo=forcePTwo-0.83;
forcePThree=forcePThree-0.75;
forcePFour=forcePFour-0.45;
forcePFive=forcePFive-0.75;
forcePSix=forcePSix-0.73;
forcePSeven=forcePSeven-0.43;
forcePEight=forcePEight-0.53;

f10cr=f10cr+1.3;
f11cr=f11cr+1.3;

ff2=forcePTwo(1:n:end);
ff3=forcePThree(1:n:end);
ff4=forcePFour(1:n:end);
ff5=forcePFive(1:n:end);
ff6=forcePSix(1:n:end);
ff7=forcePSeven(1:n:end);
ff8=forcePEight(1:n:end);

ff10=f10cr(1:n:end);
```

```
ff11=f11cr(1:n:end);


%impact point taring
g2=34.5;
g3=35;
g4=33.4;
g5=35.5;
g6=36.2;
g7=32;
g8=33.5;

g10=24.4;
g11=24.4;

x2=(linspace((15-g2),(50-g2),1000))';
x3=(linspace((15-g3),(50-g3),1000))';
x4=(linspace((15-g4),(50-g4),1000))';
x5=(linspace((15-g5),(50-g5),1000))';
x6=(linspace((15-g6),(50-g6),1000))';
x7=(linspace((15-g7),(50-g7),1000))';
x8=(linspace((15-g8),(50-g8),1000))';

x10=(linspace((22-g10),(52-g10),1000))';
x11=(linspace((22-g11),(52-g11),1000))';


xx2=x2(1:n:end);
xx3=x3(1:n:end);
xx4=x4(1:n:end);
xx5=x5(1:n:end);
xx6=x6(1:n:end);
xx7=x7(1:n:end);
```

```
xx8=x8(1:n:end);

xx10=x10(1:n:end);
xx11=x11(1:n:end);


%plotting

figure(1)
plot(x2,forcePTwo,'b--')
title('Large Indenter Plots 39K')
xlabel('displacement (mm)')
ylabel('pressure kg/mm2')
grid on
hold on

plot(x3,forcePThree,'g--')
plot(x4,forcePFour,'k--')
plot(x5,forcePFive,'b*')
plot(x6,forcePSix,'k.')
plot(x7,forcePSeven)
plot(x8,forcePEight,'r--')
plot(x10,f10cr)
plot(x11,f11cr)

legend('two','three','four','five','six','seven','Eight','then','eleven')
hold off

figure(2)
set(gcf,'position',[0 , 0 , 750 , 500])
plot(xx2,ff2,'ro')
title('Data 39K')
xlabel('Displacement (mm)')
```

```
ylabel('Pressure (kg/mm^2)')
grid on
hold on
plot(xx3,ff3,'g+')
plot(xx4,ff4,'b*')
plot(xx5,ff5,'k.')
plot(xx6,ff6,'rx')
plot(xx7,ff7,'gs')
plot(xx8,ff8,'bd')
plot(xx10,ff10,'k^')
plot(xx11,ff11,'rv')

ylim([-0.5 4])
xlim([-5 15])

legend('D=4.11mm P2','D=4.11mm P3','D=4.11mm P4','D=4.11mm P5','D=4.11mm P6','D=4.11mm
P7','D=4.11mm P8','D=2.25mm P10 Sweep','D=2.25mm P11 Sweep','location','northwest')
hold off


%%%%%%%%%%%%%%%%%%%%%%%%%%%%%%%%%%%%%%%%%%%%%%%%%%%%%%%%%%%%%%%%%%%%%%%
%average find
a=[x2(1),x3(1),x4(1),x5(1),x6(1),x7(1),x8(1),x10(1),x11(1)];
a1=max(a);
a1=-2.0;
b=[x2(end),x3(end),x4(end),x5(end),x6(end),x7(end),x8(end),x10(end),x11(end)];
b1=min(b);
b1=10;


a2=(find(x2 <= a1));
b2=(find(x2 >= b1));
f2a=forcePTwo(a2(end):b2(1));
```

```
a3=(find(x3 <= a1));
b3=(find(x3 >= b1));
f3a=forcePThree(a3(end):b3(1));

a4=(find(x4 <= a1));
b4=(find(x4 >= b1));
f4a=forcePFour(a4(end):b4(1));

a5=(find(x5 <= a1));
b5=(find(x5 >= b1));
f5a=forcePFive(a5(end):b5(1));

a6=(find(x6 <= a1));
b6=(find(x6 >= b1));
f6a=forcePSix(a6(end):b6(1));

a7=(find(x7 <= a1));
b7=(find(x7 >= b1));
f7a=forcePSeven(a7(end):b7(1));

a8=(find(x8 <= a1));
b8=(find(x8 >= b1));
f8a=forcePEight(a8(end):b8(1));

a15=(find(x10 <= a1));
b15=(find(x10 >= b1));
f15a=f10cr(a15(end):b15(1));

a16=(find(x11 <= a1));
b16=(find(x11 >= b1));
f16a=f11cr(a16(end):b16(1));
```

```
c1=[length(f2a),length(f3a),length(f4a),length(f5a),length(f6a),length(f7a),length(f8a)];
c2=[length(f15a),length(f16a)];
d1=min(c1);
d2=min(c2);
forcePTwoAvg=f2a(1:d1);
forcePThreeAvg=f3a(1:d1);
forcePFourAvg=f4a(1:d1);
forcePFiveAvg=f5a(1:d1);
forcePSixAvg=f6a(1:d1);
forcePSevenAvg=f7a(1:d1);
forcePEightAvg=f8a(1:d1);
pos6sw=f15a(1:d2);
pos7sw=f16a(1:d2);


average39klarge=(forcePTwoAvg+forcePThreeAvg+forcePFourAvg+forcePFiveAvg+forcePSixAvg
+forcePSevenAvg+forcePEightAvg)/7; %
avgx39k=(linspace(a1,b1,d1))';

avgswp=(pos6sw+pos7sw)'/2;
avgx2=(linspace(a1,b1,d2))';

figure(3)
set(gcf,'position',[0,0,600,400])
movegui('southwest')
plot(avgx39k,average39klarge,'r*')
hold on
title('Data 39K Average')
xlabel('displacement (mm)')
ylabel('pressure (kg/mm2)')
plot(avgx2,avgswp,'b.')
grid on
```

```
legend('Average 4.11mm dia','Average 2.25mm dia','location','northwest')
hold off

figure(4)
set(gcf,'position',[0,0,600,400])
movegui('southeast')
plot(avgx39k,forcePTwoAvg)
hold on
plot(avgx39k,forcePThreeAvg)
plot(avgx39k,forcePFourAvg)
plot(avgx39k,forcePFiveAvg)
plot(avgx39k,forcePSixAvg)
plot(avgx39k,forcePSevenAvg)
plot(avgx39k,forcePEightAvg)
grid on
legend
```

Appendix D - Arduino Example Code

Included below is an example of Arduino code used, this code integrates the load cell amplifier, motor control and control buttons.

```
#include <HX711.h>

HX711 scale;

float calibration_factor = 149;  // sets calibration factor

float force;


const int stepPin=2;     // pin for stepper pulsing

const int dirPin=3;      // controles step direction, connect to buttons

const int enablePin=4;   // enable stepper drive

const int buttonUp= 10;  // attach pin for UP button

const int buttonDown=11; // attach pin for DOWN button

long previousMillis = 0; // store last time of update

long interval = 10;     // interval of pulsing

int pulseOn = LOW;       // start pulse state

int goingUp = 0;         // going up button

int goingDown =0;        // going down button

long pulseCounter =0;     // counter for number of pulses, for distance calculation

int i=1;                 // counter for number of loops before

int x=1;                  // counter doesn't check things every loop

const int ms1=7;         // microstepping pin 1
```

```
const int ms2=8;         // microstepping pin 2
const int ms3=9;         // microstepping pin 3



void setup() {
Serial.begin(9600); //sets the serial baud rate
scale.begin(5,6);

scale.set_scale(calibration_factor); //Adjust to this calibration factor

scale.tare();
long zero_factor = scale.read_average();

pinMode(stepPin,OUTPUT);
pinMode(dirPin,OUTPUT);
pinMode(enablePin,OUTPUT);
  pinMode(buttonUp,INPUT);
pinMode(buttonDown,INPUT);
pinMode(ms1,OUTPUT);
pinMode(ms2,OUTPUT);
pinMode(ms3,OUTPUT);
}
```

```
void loop() {


  digitalWrite(ms1,HIGH);
digitalWrite(ms2,HIGH);
digitalWrite(ms3,HIGH);


  //reads button pins and sets enable and direction pins to corrent direction


if (x>20)  {
goingUp= digitalRead(buttonUp);
goingDown=digitalRead(buttonDown);
//force=scale.get_units(),5;  //get force data


  if(goingUp==HIGH){
  digitalWrite(enablePin,LOW);
  digitalWrite(dirPin,HIGH);
  //Serial.println("going up ");
  }
  if (goingDown==HIGH) {
  digitalWrite(enablePin,LOW);
  digitalWrite(dirPin,LOW);
  //Serial.println("going down ");
  }
```

```
  if (goingDown==LOW && goingUp==LOW) {
    digitalWrite(enablePin,HIGH);
    }
    x=0;
}
i++ ;
if (i >1000) {

delay(50);
Serial.print(scale.get_units(),5);
Serial.print(",");
Serial.print(pulseCounter);
Serial.println();
i=0;
}



// stepper pulsing, try to do outside of button section to simplify code looping, will need to
//check if the counting and outputing is accurate

if ( (millis() - previousMillis) > interval && pulseOn == LOW) {
   previousMillis = millis();
```

```
    pulseOn = HIGH;
   digitalWrite(stepPin,HIGH);
   //Serial.println("high");

   x++;
}
else if ((millis() - previousMillis) > interval && pulseOn == HIGH ){

  pulseOn = LOW;
  //Serial.println("low");
  digitalWrite(stepPin,LOW);

}
// counter for number of steps

if (goingUp == HIGH)
{
pulseCounter = pulseCounter +x ;
}
if (goingDown == HIGH){
pulseCounter = pulseCounter -x ;
}
```